SIAM J. APPL. MATH.
Vol. 66, No. 6, pp. 1917–1948

RETURN MAP CHARACTERIZATIONS FOR A MODEL OF BURSTING WITH TWO SLOW VARIABLES*

ROGER E. GRIFFITHS† AND MARK PERNAROWSKI‡

Abstract. Various physiological systems display bursting electrical activity (BEA). There exist numerous three-variable models to describe this behavior. However, higher-dimensional models with two slow processes have recently been used to explain qualitative features of the BEA of some experimentally observed systems [T. Chay and D. Cook, *Math. Biosci.*, 90 (1988), pp. 139–153; P. Smolen and J. Keizer, *J. Memb. Biol.*, 127 (1992), pp. 9–19; R. Bertram et al., *Biophys. J.*, 79 (2000), pp. 2880–2892; R. Bertram et al.,, *Biophys. J.*, 68 (1995), pp. 2323–2332; J. Keizer and P. Smolen, *Proc. Nat. Acad. Sci. USA*, 88 (1991), pp. 3897–3901]. In this paper we present a model with two slow and two fast variables. For some parameter values the system has stable equilibria, while for other values there exist bursting solutions. Singular perturbation methods are used to define a one-dimensional return map, wherein fixed points correspond to singular bursting solutions. We analytically demonstrate that bursting solutions may exist even with a combination of activating and inactivating slow processes. We also demonstrate that for different parameters, bursting solutions may coexist with stable equilibria. Hence small variations in the initial conditions may drastically affect the dynamics.

Key words. bursting, return map, singular perturbation solutions

AMS subject classifications. 34A, 34C15, 34C29, 34D15, 34E15

DOI. 10.1137/050635201

1. Introduction.

Bursting electrical activity (BEA) is a phenomenon in which the membrane potential of a cell goes through a succession of alternating active (spiking) and silent states (cf. Figure 1.1). Such patterns of electrical activity were first observed experimentally in the electrical activity of the Aplysia R-15 neuron [52, 1]. Biophysical mechanisms of bursting in the pancreatic β-cell were proposed by Atwater et al. [2], which were later used by Chay and Keizer [15] to create the first "minimal" mathematical model based on the Hodgkin–Huxley model. Since then, there have been a large number of β-cell models [14, 27, 31, 46, 32, 13, 49] and other cellular models exhibiting bursting behavior [18, 26, 56, 55, 8, 33].

Most mathematical models of BEA are variants of the Hodgkin–Huxley model [29] of the squid giant axon. Generically, these models make up a set of (dimensional) differential equations,

$$C_m \frac{dv}{dt} = -\sum_X I_X(v,z), \tag{1.1}$$

$$\frac{dz_i}{dt} = \frac{(z_{i\infty}(v) - z_i)}{\tau_i(v)}, \quad i = 1, 2, \ldots, n, \tag{1.2}$$

where t is time, v is the transmembrane potential, and z_i are typically channel activation (resp., inactivation) variables. In some instances, z_i may be concentrations of regulatory chemicals. Regardless, all such models have a current balance equation

*Received by the editors July 5, 2005; accepted for publication (in revised form) May 10, 2006; published electronically September 12, 2006.
http://www.siam.org/journals/siap/66-6/63520.html
†Department of Mathematics, Mercyhurst College, Erie, PA 16546 (rgriffiths@mercyhurst.edu).
‡Department of Mathematical Sciences, Montana State University, Bozeman, MT 59717 (pernarow@math.montana.edu).

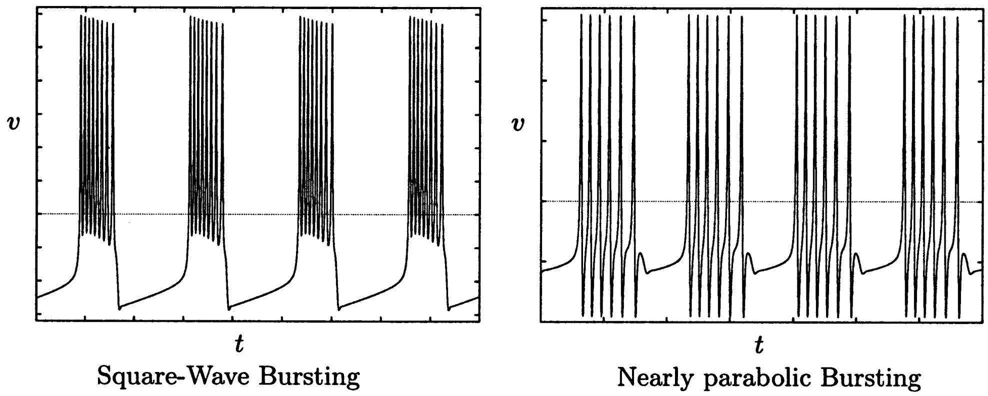

FIG. 1.1. *Some examples of bursting, with their classification type indicated. Here voltage v is plotted against time t.*

such as (1.1), where C_m is the cell's total capacitance and I_X are currents (of type X, i.e., voltage-gated calcium) thought to be relevant to the particular cell being examined. In models of BEA, the time constants τ_i often have greatly different magnitudes. Thus, from a modeling (resp., mathematical) perspective, bursting depends on processes with distinctly different time scales, typically termed *fast* and *slow*. The fast processes remain in quasi-steady state except for the rapid transitions between states, while the slow processes modulate the fast dynamics between the silent and active states.

The nonlinearities essential in biophysical models of bursting such as (1.1)–(1.2) make any form of analysis difficult. Consequently, phenomenological models have often been used to explore issues related to bursting (see Hindmarsh and Rose [28], Pernarowski [36], Baer, Rinzel, and Carrillo [3]). Regardless of what type of model is studied, the vast majority of models involve multiple time scales and can be written as a system of the form

$$\frac{dx}{dt} = f(x,y)\,, \quad x \in \mathbb{R}^2, \tag{1.3}$$

$$\frac{dy}{dt} = \varepsilon g(x,y)\,, \quad y \in \mathbb{R}^K, \tag{1.4}$$

where $\varepsilon \ll 1$ is a small parameter. Cast in this form, x are fast variables, while y are slow variables.

Many models of BEA consisting of one slow variable ($K = 1$) have been studied. The goals of such studies have varied. Some studies use numerical methods to simulate postulated models to explain cell mechanisms. Such is the case in numerous studies of the insulin-secreting pancreatic β-cell [15, 12, 46, 45, 43, 17, 44]. In other studies, the goal has been to use singular perturbation ideas and methods to classify the different type of oscillations which can arise from such systems. Such classification studies originated with work by Rinzel [41] and were subsequently continued by others [36, 4, 16, 30]. Lastly, other studies have focused on proving the existence of periodic bursting orbits. For instance, Terman [53] formalized the singular perturbation construction. Interest in such fast-slow systems with one slow variable has even spawned studies of topological-based proof techniques [24].

Other models of BEA have more than one slow variable [14, 49, 5, 32, 6, 40]. In some recent studies, bursting cycles have been characterized using two-dimensional maps to aid in the construction of singular solutions [51, 9]. In other recent works, one-dimensional maps have been used to explore bifurcations in systems with one slow variable [34]. In all of these works, periodic bursting cycles equate to fixed points of the map, making the use of the map construct simplistically elegant. Despite such recent uses of maps to describe bursting cycles, explicit singular perturbation and numerical constructions of the maps for models exhibiting bursting remain scant.

In this paper we study a phenomenological model of bursting with two slow variables. As in previous works, singular perturbation methods are used here to define a return map to describe the bursting cycle. Unlike previous analyses of models having two slow and two fast variables, our return map is one-dimensional. Also, because the model is simple, many of the perturbation calculations can be performed analytically. The goal of this work is three-fold: (1) to outline new analytical and numerical techniques for such singular constructions; (2) to analytically demonstrate that bursting solutions can exist even when the slow processes are activating and inactivating; and (3) to demonstrate that bursting solutions can coexist with stable equilibria. The latter result, for example, can be used to explain why some isolated pancreatic β-cells burst while others do not [50]. The implications and importance of these results are discussed in the conclusion.

In section 2, the model is introduced and its leading-order fast, slow, and averaged fast subsystems are defined. Since the model is an extension of a previously studied model [36, 37, 16], stability analyses related to the fast subsystem are referenced. A detailed multiple scales averaging calculation used to derive the averaged fast subsystem in section 2 is included in an appendix. This derivation is a multivariable generalization of the single slow variable derivation presented in [39].

As each of the slow and averaged fast subsystems is two-dimensional, each defines a two-dimensional map between the transition curves[1] between the silent and active phases. These maps and their dimensionality reduction are carefully defined in section 3. Singular bursting solutions are determined by the fixed points of the composition ϕ of these maps.

When the time constants $\tau_i, i = 1, 2$, of the slow variables are equal, a transformation is used in section 4 to demonstrate that the model dynamics can be described by a single slow variable. As a consequence, singular bursting solutions exist even if one slow variable is activating and the other is inactivating. Furthermore, we show that the map ϕ defined in section 3 can be computed explicitly. However, when the time constants τ_i are not equal, these analyses do not apply. For this case, a numerical method for computing ϕ is developed and implemented in section 5. The method uses AUTO [19] to solve two one-parameter families of boundary value problems whose solutions can then be used to construct ϕ.

Lastly, in section 6, we present numerical simulations which demonstrate that for certain parameter values the model exhibits bistability between stable equilibria and bursting solutions. There, this dynamic is shown to relate to the domains of the maps used to construct the singular bursting solutions.

[1]Saddle-node and homoclinic bifurcation curves of the fast subsystem.

2. Model and subsystem definitions. In this paper we will study the following two slow variable models:

$$\frac{d\mathbf{u}}{dt} = \mathbf{F}(\mathbf{u}, \mathbf{z}) = \begin{pmatrix} f(u) - w - x - \gamma y \\ g(u) - w \end{pmatrix}, \tag{2.1}$$

$$\frac{d\mathbf{z}}{dt} = \varepsilon \mathbf{G}(\mathbf{u}, \mathbf{z}) = \varepsilon \begin{pmatrix} \frac{h_1(u) - x}{\tau_1} \\ \frac{h_2(u) - y}{\tau_2} \end{pmatrix}, \tag{2.2}$$

where $0 < \varepsilon \ll 1$, $\mathbf{u} = (u, w)^T$ are fast variables and $\mathbf{z} = (x, y)^T$ are slow variables.

In the model, τ_1, τ_2, and γ are constants; the equations

$$f(u) = -\frac{a}{3}u^3 + a\mu u^2 + (1 - a(\mu^2 - \eta^2))u\,, \tag{2.3}$$

$$g(u) = \left(1 - \frac{a}{3}\right)u^3 + a\mu u^2 - (2 + a(\mu^2 - \eta^2))u - 3 \tag{2.4}$$

are the same functions used in [36, 37], and (a, μ, η) are parameters. The complicated form of the polynomials f and g is due in part to their derivation from a Liénard form in Pernarowski [37]. An advantage of the Liénard form is the availability of the Melnikov theory to analytically approximate homoclinic bifurcation points [39, 36]. Also, as shall be seen in the next section, the location of the fast subsystem equilibria does not depend on (a, μ, η). We mention these facts here for reference purposes only, and will not need them in subsequent analysis.

Finally,

$$h_i(u) = \beta_i(u - \alpha_i), \quad i = 1, 2, \tag{2.5}$$

where α_i and β_i are also constants.

In this model u should be interpreted as the membrane potential, whereas w is a fast conductance and x, y are slow conductances for gating channels of the same ion. Hereafter we shall refer to (2.1)–(2.2) as (FULL). Lastly, we note that throughout this paper the notation $\dot{(\ )}$ will be used to denote differentiation in t, as in $\dot{u} = \frac{du}{dt}$.

In the next few sections the fast subsystem (FS), slow subsystem (SS) and averaged fast subsystem (AFS) associated with (FULL) will be defined. These preliminary definitions will be needed to accurately define the return map in section 3.

2.1. (FS) dynamics. On the fast t time scale the dynamics of (FULL) is governed by the (FS) obtained by letting $\varepsilon = 0$,

$$\frac{du}{dt} = f(u) - w - z\,, \quad z \equiv x + \gamma y\,, \tag{2.6}$$

$$\frac{dw}{dt} = g(u) - w\,, \tag{2.7}$$

with the slow variables x and y treated as parameters and combined as shown above. In Figure 2.1 we show a numerically generated (FS) bifurcation diagram in $z = x + \gamma y$. The projection of the equilibria of (FS) onto the (u, z)-plane yields a Z-shaped curve

$$z = G(u) \equiv f(u) - g(u) = -u^3 + 3u + 3. \tag{2.8}$$

Note here that despite the dependence of f and g on the fast parameter set $\lambda_f = (a, \mu, \eta)$, G depends on no parameters. For the remainder of this paper we fix these

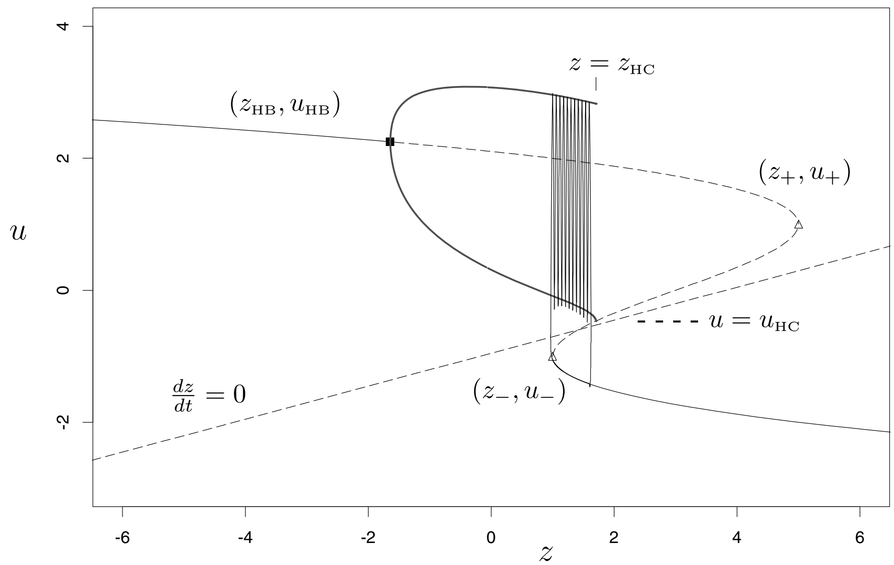

FIG. 2.1. *(FS) bifurcation diagram for* (2.6)–(2.7) *when* $\lambda_f = (a, \eta, \mu) = (\frac{1}{4}, \frac{3}{4}, \frac{3}{2})$ *with a bursting solution superimposed. Other parameter values for this illustration are* $\beta = 4, \alpha = -0.954, \varepsilon = 0.0025$.

fast-parameter values at $(a, \mu, \eta) = (\frac{1}{4}, \frac{3}{4}, \frac{3}{2})$; for details on fast parameter selection, see [36].

In Figure 2.1, solid lines on the $z = G(u)$ equilibria curve indicate stable equilibria, whereas the dashed portion indicates unstable equilibria. Equilibria on the lower branch are stable nodes, whereas equilibria on the middle branch are saddle points. The stability of the steady states on the upper branch changes at a supercritical Hopf bifurcation at $z = z_{\rm HB}$. Though Figure 2.1 was computed numerically using XPPAUT [21], the aforementioned stabilities and bifurcations were proven analytically in [36]. Stable periodic orbits (the dark, thick lines) emanate from the Hopf point and terminate at a homoclinic bifurcation on the middle branch at $z = z_{\rm HC}$. The upper and lower portions indicate the extreme values of u on the limit cycles of the (FS). Saddle-node bifurcations are indicated at $z = z_-$ and $z = z_+$. Note that the (FS) has a region of bistability, where stable lower branch equilibria and periodic orbits coexist for $z \in (z_-, z_{\rm HC})$. In later sections we will make reference to the values $u_+, u_-, u_{\rm HC}$ as the u value at which the upper saddle-node, lower saddle-node, and homoclinic bifurcations occur, respectively. Also, as indicated in Figure 2.1, when we refer to $u_{\rm HC}$ we mean the u value on the middle branch when $z = z_{\rm HC}$.

The (FS) bifurcation diagram in z described above is identical to that of the one slow variable model discussed in [37]. In that model, z evolves according to the differential equation

$$\frac{dz}{dt} = \varepsilon(h(u) - z), \tag{2.9}$$

where $h(u) = \beta(u - \alpha)$; α and β are parameters; and $\beta > 0$. Collectively, (2.6), (2.7), and (2.9) define the one slow variable model in [37]. Before we examine bursting solutions of (FULL), we briefly describe a bursting cycle of the aforementioned one slow variable model for comparison. Toward this end, the z (slow) nullcline associated with (2.9) is superimposed on the (FS) bifurcation diagram in Figure 2.1 (dashed line passing through the middle branch of the Z curve). Here we have used the slow parameter values $(\alpha, \beta) = (-0.954, 4)$.

In this example with $\beta > 0$, $\dot{z}$ is negative only below the nullcline. Thus, z slowly increases above the nullcline and decreases below it. Keeping this in mind, a bursting solution of the one slow variable model (2.6), (2.7), (2.9) is superimposed on the (FS) bifurcation diagram in Figure 2.1. In what is often referred to as the "silent phase," trajectories lie close to the lower branch of equilibria. Since $\dot{z} < 0$ on the lower branch, trajectories move to the left until bistability is lost at the saddle-node bifurcation point (z_-, u_-). As z decreases below z_-, trajectories are then attracted to the (FS) limit cycles, initiating the "active phase" marked by high-frequency oscillations. In the active phase, $\dot{z} > 0$ so that solutions slowly drift to the right until bistability is lost at the homoclinic bifurcation point at $z = z_{\text{HC}}$. Trajectories are then attracted to the lower branch, initiating the silent phase again.

This explanation of the resulting "square wave" bursting cycle was given by Rinzel in [41], where he classified several other types of bursting cycles depending on their fast (and slow) subsystem structure. In a later classification scheme [4], the cycle depicted in Figure 2.1 is known as type I bursting. In a subsequent and more extensive classification scheme [30], the same cycle is described as a "fold/homoclinic burster"; its name is due to the fact that the silent phase ends via a *fold* bifurcation and the active phase terminates via a saddle *homoclinic* orbit bifurcation.

Though the (FS) of (FULL) is identical to that of the one slow variable model just discussed, in (FULL) the slow variables x and y do not evolve according to (2.9) but by (2.2). Instead, silent phase trajectories of (FULL) are attracted to the stable manifold

$$\mathbb{S}_L = \{(u, w, x, y) : x + \gamma y = G(u), w = g(u), u < u_-\}, \tag{2.10}$$

formed by the lower branch equilibria of the (FS). In contrast to the single slow variable model, this is a two-dimensional manifold in $\mathbb{R}^4$, making the preceding explanation of the bursting cycle using (2.9) inapplicable. Later, we shall make use of the fact that bursting cycles of (FULL) are conveniently described by projecting them onto the (x, y)-plane. Toward this end, we define the projection $P(\mathbb{S}_L)$ of $\mathbb{S}_L$ onto the (x, y)-plane as

$$S_L = \{(x, y) : x + \gamma y = G(u), u < u_-\}. \tag{2.11}$$

The reason we distinguish S_L from $\mathbb{S}_L$ is that later it will become easier to visualize trajectories on S_L rather than on $\mathbb{S}_L$. We note, for instance, that equilibria of (FULL) truly exist only on $\mathbb{S}_L$.

2.2. (SS) dynamics. In this section we define the (SS) of (FULL). Using the (slow time) transformation $\tau = \varepsilon t$ in (FULL) and then setting $\varepsilon = 0$ results in the system

$$z = x + \gamma y = G(u), \tag{2.12}$$

$$w = g(u), \tag{2.13}$$

$$\frac{dx}{d\tau} = \frac{h_1(u) - x}{\tau_1}, \tag{2.14}$$

$$\frac{dy}{d\tau} = \frac{h_2(u) - y}{\tau_2}. \tag{2.15}$$

Collectively, (2.12)–(2.15) define the (SS) of (FULL) as long as $u < u_-$. Solutions of (2.12)–(2.15) yield trajectories on $\mathbb{S}_L$ which are leading-order approximations to the silent phase of (FULL).

Equations (2.12)–(2.13) are algebraic conditions which ensure the (SS) flow remains on $\mathbb{S}_L$. Rewritten, this condition is equivalent to the cubic

$$u^3 - 3u - 3 + z = 0. \tag{2.16}$$

Roots of (2.16) can be explicitly computed. Here we use the trigonometric form of these roots discussed in [7]. Since the root associated with $\mathbb{S}_L$ has $u < u_-$, it is readily verified that on the lower branch of the (FS),

$$u = u_{\text{LB}}(z) = \begin{cases} 2\cos\left(\frac{1}{3}\arccos\left(\frac{3-z}{2}\right) + \frac{2\pi}{3}\right), & 1 \le z \le 5, \\ -2\cosh\left(\frac{1}{3}\ln\left(\frac{z-3}{2} + \sqrt{\left(\frac{z-3}{2}\right)^2 - 1}\right)\right), & z > 5. \end{cases} \tag{2.17}$$

This allows one to rewrite (2.14)–(2.15) as

$$\frac{dx}{d\tau} = F_1(x,y) \equiv \frac{\beta_1(u_{\text{LB}}(z) - \alpha_1) - x}{\tau_1}, \tag{2.18}$$

$$\frac{dy}{d\tau} = F_2(x,y) \equiv \frac{\beta_2(u_{\text{LB}}(z) - \alpha_2) - y}{\tau_2}. \tag{2.19}$$

Solutions of (2.18)–(2.19) are leading-order silent phase approximations of (FULL) projected onto the (x, y)-plane when initial conditions are close to $\mathbb{S}_L$. In section 3, system (2.18)–(2.19) will be used to define the portion of the map needed to describe the dynamics of (FULL) in the silent phase.

At this point we also note that the (FS) and the (SS) depend on different parameters. For future reference, we define the *fast* parameter set λ_f as those parameters which occur explicitly in the (FS) but not in the (SS). In this case, $\lambda_f = (a, \eta, \mu)$. In a similar fashion, we define the *slow* parameter set λ_s as those parameters which occur explicitly in the (SS) but not in the (FS). For (FULL), $\lambda_s = (\beta_1, \beta_2, \alpha_1, \alpha_2, \tau_1, \tau_2)$.

2.3. (AFS). In this section we define the (AFS) associated with (FULL). Like the (SS), the (AFS) is a leading-order approximation for the x and y components of (FULL) valid for slow times $\tau = O(1)$. In contrast to the (SS), the (AFS) is an approximation valid only for initial conditions near the (FS) limit cycles.[2] The details of the expansions, assumptions, and multiple scales procedure used to derive the (AFS) are included in the appendix. Here we merely summarize the relevant points.

Defining the set

$$S_A = \{(x,y) : z_{HB} < x + \gamma y < z_{\text{HC}}\}, \tag{2.20}$$

we note from Figure 2.1 that the (FS) has a stable $T(z)$-periodic limit cycle $(u, w) = \Omega(t, z)$ for every $(x, y) \in S_A$. Here the limit cycle $\Omega(t, z)$ and its associated period T

[2] Since the averaging is performed over these (FS) limit cycles, we named the system the "averaged fast subsystem." This naming scheme was chosen to avoid confusion were the averaging performed over periodic orbits lying near the slow manifold of the (SS). Indeed, in [25], the (SS) is shown to possess Hopf bifurcations for some parameter values. An exploration of averaged slow subsystems near such Hopf points is not done in this paper.

are functions of $z = x + \gamma y$ alone. If we define the average

$$\hat{u}(z) \equiv \frac{1}{T(z)} \int_0^{T(z)} \Omega_1(\eta, z) d\eta, \tag{2.21}$$

where $\Omega(t, z) = (\Omega_1(t, z), \Omega_2(t, z))$, and take advantage of the linearity of $h_i(u)$, $i = 1, 2$, in u, the (AFS) of (FULL) is

$$\frac{dx}{d\tau} = \widehat{G}_1(x, y) = \frac{h_1(\hat{u}(x + \gamma y)) - x}{\tau_1}\ , \tag{2.22}$$

$$\frac{dy}{d\tau} = \widehat{G}_2(x, y) = \frac{h_2(\hat{u}(x + \gamma y)) - y}{\tau_2}\ . \tag{2.23}$$

For initial conditions sufficiently close to Ω, solutions of (2.22)–(2.23) are leading-order asymptotic approximations of (x, y) in (FULL) for times $\tau = O(1)$ as long as $(x(\tau), y(\tau)) \in S_A$. In the singular limit, bistability of the (FS) is lost when $z = z_{\mathrm{HC}}$, at which point a transition to the silent phase occurs.

Subsequently, we will need to perform computations using the (AFS). For these calculations we used AUTO [19] to compute $\hat{u}(z)$ for a range of z values. These values are shown in Figure 2.2, where they are compared to an approximating function $\hat{u}_a(z)$ of the form

$$\widehat{u}_a(z) = u_{\mathrm{HC}} + a_0 \left(z_{\mathrm{HC}} - z\right)^{\frac{1}{p}} + a_1 \left(z_{\mathrm{HC}} - z\right). \tag{2.24}$$

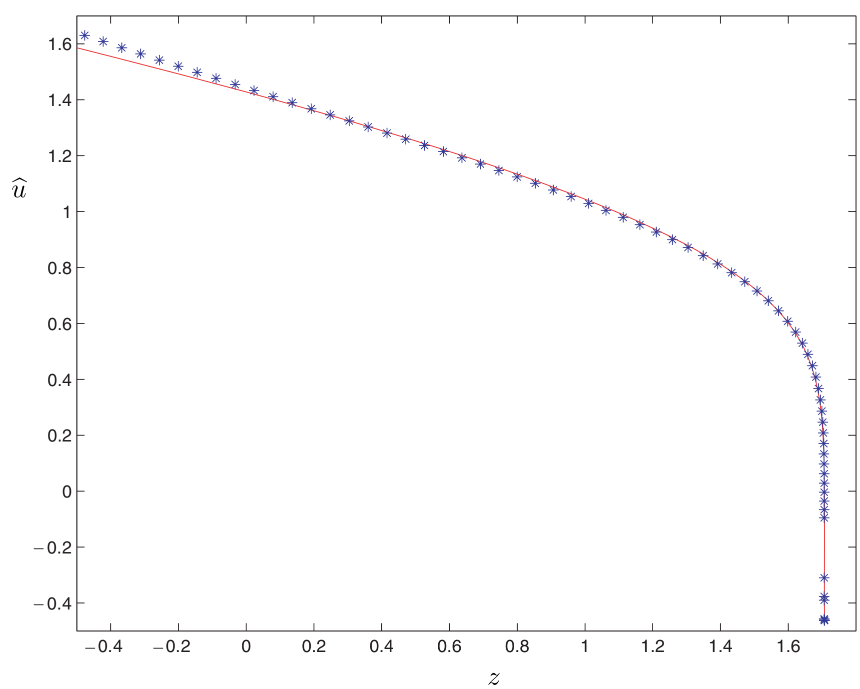

FIG. 2.2. *$\widehat{u}(z)$ plotted as AUTO-generated data along with the approximating function $\widehat{u}_a(z)$. $\widehat{u}(z)$ is u averaged over the limit cycles $\Omega(t, z)$. The AUTO-generated data are plotted as *'s and the superimposed curve is the approximating function $\widehat{u}_a(z)$ defined in (2.24).*

As can be seen in Figure 2.2, for the choice $(p, a_0, a_1) = (8, 1.378, 0.260)$, $\hat{u}(z)$ and $\hat{u}_a(z)$ are almost indistinguishable over the active phase range $z_- < z < z_{\text{HC}}$. Here $z_- = 1$ and $(z_{\text{HC}}, u_{\text{HC}}) \simeq (1.70633, -0.46466)$ were estimated using AUTO. We note that (2.24) may be viewed as a two term asymptotic expansion for $\hat{u}(z)$. However, we currently have no theoretical explanation as to why $\hat{u}_a(z)$ approximates $\hat{u}(z)$ so well.

We conclude this section with a numerical example showing how well the (AFS) approximates (FULL) in the active phase. In Figure 2.3, an active phase trajectory of (FULL) projected into the (x, y)-plane is shown together with a solution of the (AFS) with the same initial conditions. Superimposed is the line $x + \gamma y = z_{\text{HC}}$, labeled as Γ_{HC} in the figures. On this line the (FS) has a homoclinic bifurcation. For the

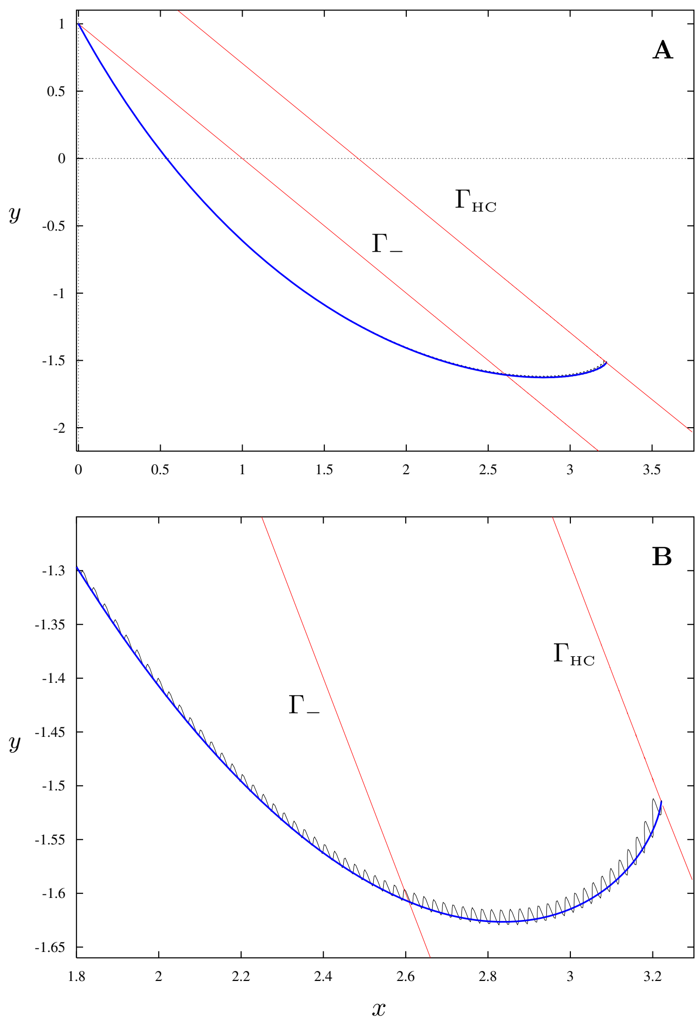

Fig. 2.3. *Both figures show an active phase trajectory of (FULL) projected into the (x, y)-plane along with the (AFS) approximation using* (2.24)*,* $\lambda_s = (\beta_1, \beta_2, \alpha_1, \alpha_2, \tau_1, \tau_2) = (4, -1, -1, -0.7, 1, 0.5)$*, and* $\varepsilon = 0.0025$*.* **A** *shows the entire active phase, whereas in* **B** *we have enlarged the region near the jump to the silent phase at the homoclinic bifurcation of the (FS). The lines* Γ_{HC} *and* Γ_- *are defined in* (3.1), (3.2)*, respectively.*

(x, y) values above Γ_{HC} the (FS) does not have periodic orbits. Thus, for those values the (AFS) is undefined. Moreover, to leading order, as trajectories of (FULL) cross above Γ_{HC}, a rapid transition back to the silent phase occurs. Analogous transitions of (FULL) from the silent phase into the active phase would occur as trajectories traverse below the line $x + \gamma y = z_-$. This line, labeled as Γ_-, is also superimposed in the figures purely for reference purposes and represents the (x, y) pairs for which the (FS) has a saddle-node bifurcation. A more complete discussion of these transition curves and their relevance to an overall bursting cycle is relegated to the next section, where the return maps for the leading dynamics are defined. Here, the point is simply to illustrate just how well the (AFS) using (2.24) approximates (FULL) in the active phase. In this particular example, parameter values were chosen so that the projected active phase solution of (FULL) extended over a wide range of $z = x + \gamma y$ for which the (FS) has limit cycles. The figures illustrate that the projected trajectory $(x(t), y(t))$ of (FULL) is very well approximated by the (AFS) trajectories over just such a large range of z values. Indeed, even in the enlargement shown in Figure 2.3B, the trajectories remain very close in the region between Γ_- and Γ_{HC}, where the (FS) is bistable.

3. Definition of the return map.

We define a bursting solution of (FULL) as a trajectory which both is periodic and traverses the active and silent phases once during each period. By a singular bursting solution of (FULL) we mean a bursting solution whose leading-order approximation consists of a silent phase portion approximated by the (SS), an active phase portion approximated by the (AFS), and two rapid transitions between each phase at $z = z_-$ and $z = z_{\text{HC}}$, as illustrated in Figure 2.1.

The return map we construct to describe singular bursting solutions of (FULL) is actually the composition of two maps, as illustrated in Figure 3.1. One map accounts for the silent phase and the other for the active phase. The silent phase portion of the singular solution is constructed from a trajectory $\tilde{\gamma}_x(\tau)$ of the (SS) which starts at $\mathbf{X} = (x, y)$ on the curve

$$\Gamma_{\text{HC}} = \{(x, y) : x + \gamma y = z_{\text{HC}}\} \subset \overline{S}_A \tag{3.1}$$

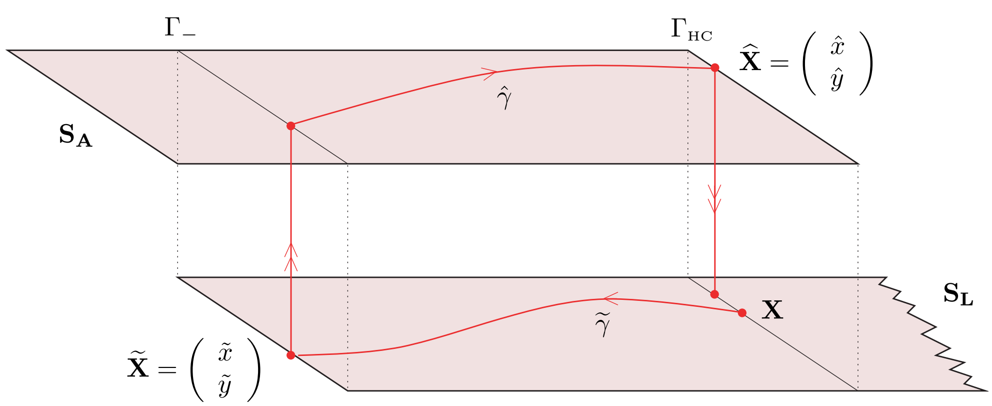

FIG. 3.1. *Illustration of the return map definition for singular bursting solutions. Illustration S_L is shown on bottom with a trajectory of the (SS) $\tilde{\gamma}$ beginning at $\mathbf{X} = (x, y) \in \Gamma_{HC}$. After a fast transition to S_A on the top, the (AFS) trajectory $\hat{\gamma}$ is shown to terminate at $\widehat{\mathbf{X}} \in \Gamma_{HC}$.*

and terminates at $\widetilde{\mathbf{X}}$ on

$$\Gamma_- = \{(x,y) : x + \gamma y = z_-\} \subset \overline{S}_A \tag{3.2}$$

after time T_s. When such transitions occur, this defines a map $\widetilde{\Phi} : \Gamma_{\text{HC}} \to \Gamma_-$ such that $\widetilde{\mathbf{X}} = \widetilde{\Phi}(\mathbf{X})$.

Similarly, the active phase portion is constructed from a trajectory $\hat{\gamma}_x(\tau)$ of the (AFS) which starts at $\widetilde{\mathbf{X}}$ on the lower saddle-node curve Γ_- and terminates at $\widehat{\mathbf{X}}$ on the curve Γ_{HC}, which forms a boundary of S_A. This transition defines a map $\widehat{\Phi} : \Gamma_- \to \Gamma_{\text{HC}}$ such that $\widehat{\mathbf{X}} = \widehat{\Phi}(\widetilde{\mathbf{X}})$.

The composition of these two maps may be written as $\Phi : \Gamma_{\text{HC}} \to \Gamma_{\text{HC}}$, $\mathbf{X} = (x, y)$,

$$\Phi(\mathbf{X}) = \left(\widehat{\Phi} \circ \widetilde{\Phi}\right)(\mathbf{X}). \tag{3.3}$$

Given these definitions, there is then a 1-1 correspondence between singular bursting solutions and fixed points of Φ.

At this point we also remark that $\widetilde{\Phi}$ and $\widehat{\Phi}$ are, technically, maps from $\mathbb{R}^2$ into $\mathbb{R}^2$, but they have restricted domains, i.e., $\Gamma_{\text{HC}} \subset \mathbb{R}^2$ for $\widetilde{\Phi}$. Clearly such domain restrictions are not needed. For instance, one could have defined $\widetilde{\Phi}$ as the flow function associated with the (SS) defined on $D_\Phi = \{(x,y) : x + \gamma y > z_-\}$. Although such a definition has much theoretical appeal, our subsequent dimensionality reduction below is slightly more transparent using the domain restrictions.

A feature we use to our advantage is that y is a function of x on both Γ_- and Γ_{HC}—specifically, on Γ_-: $y = \frac{z_- - x}{\gamma}$ and on Γ_{HC}: $y = \frac{z_{\text{HC}} - x}{\gamma}$. As such, $\widehat{\Phi}$ reduces to a one-dimensional map $\widehat{\phi} : \mathbb{R} \to \mathbb{R}$, $\widehat{\phi}(x_0) = \hat{x}(T_a)$, where T_a is the active phase duration. Here $\widehat{x}_0 = \widehat{\phi}(x_0)$ is the x-coordinate of an (AFS) trajectory, where bistability is lost at $z = z_{\text{HC}}$ and a transition to the silent phase occurs. Adopting this convention, the domain of the map $\widehat{\phi}$ can be written

$$D(\widehat{\phi}) = \{x \in \mathbb{R} \mid \exists T_a < \infty \ni \widehat{\gamma}_x(T_a) \cap \Gamma_{\text{HC}} \neq \emptyset\},$$

where $\emptyset$ is the empty set.

An analogous one-dimensional map for the (SS) may be defined. Again exploiting the functional relationship of x and y on Γ_{HC} and Γ_-, we define the map $\widetilde{\phi} : \mathbb{R} \to \mathbb{R}$ with domain

$$D(\widetilde{\phi}) = \{x \in \mathbb{R} \mid \exists T_s < \infty \ni \widetilde{\gamma}_x(T_s) \cap \Gamma_- \neq \emptyset\},$$

where T_s is the silent phase duration.

Then, as with the map Φ, there is a 1-1 correspondence of singular bursting solutions and fixed points $\bar{x}$ of the map

$$\phi(x) = (\widehat{\phi} \circ \widetilde{\phi})(x), \quad x \in D(\phi) = \{x \in \mathbb{R} \mid x \in D(\widetilde{\phi}),\ \widetilde{\phi}(x) \in D(\widehat{\phi})\}.$$

Domain issues associated with the map are complicated, but some will be addressed in section 6. If $R(\widehat{\phi})$ is the range of $\widehat{\phi}$, then, given our previous definitions, the set $W \equiv R(\widehat{\phi}) \cap D(\widetilde{\phi})$ could be empty, equal to $D(\widetilde{\phi})$, or a (nonempty) strict subset of $D(\widetilde{\phi})$. In the next section we show that for a subset of slow parameter space, singular bursting solutions exist and W is nonempty. The case when W is a strict subset of $D(\widetilde{\phi})$ relates to bistability between bursting solutions and stable equilibria on $\mathbb{S}_L$. This will be discussed in section 6.

4. Degenerate case. In this section we examine a degenerate case of (FULL), where the time constants τ_1 and τ_2 are equal. In this degenerate case, (FULL) is shown to have a three-dimensional manifold on which (for certain parameter values) bursting solutions exist. Furthermore, we explicitly compute the maps defined in the previous section and the fixed point of ϕ associated with the singular bursting solution.

We accomplish these goals using the following linear transformation of the slow variables:

$$\mathbf{p} = A\mathbf{z} + \mathbf{b} = \begin{bmatrix} a_{11} & a_{12} \\ 1 & \gamma \end{bmatrix} \begin{pmatrix} x \\ y \end{pmatrix} + \begin{pmatrix} b_1 \\ 0 \end{pmatrix}, \quad \mathbf{z} = (x, y)^T, \tag{4.1}$$

where $\mathbf{p} = (p, z)^T$ are the new slow variables, $z = x + \gamma y$ are as before, and a_{11}, a_{12}, b_1 are to be determined. Since z is one of the new variables, the new (FS) of the transformed (FULL) will depend solely on z. Assuming $a_{11}\gamma - a_{12} \neq 0$ so that A is invertible, (4.1) and (2.2) imply

$$\frac{d\mathbf{p}}{dt} = \varepsilon A \mathbf{G}\left(u, A^{-1}(\mathbf{p} - \mathbf{b})\right). \tag{4.2}$$

Since $\mathbf{G}(u, \mathbf{z})$ depends linearly on u, x, and y, (4.2) can be equivalently written as

$$\frac{d\mathbf{p}}{dt} = \begin{bmatrix} \eta_{11} & \eta_{12} & \eta_{13} \\ \eta_{21} & \eta_{22} & \eta_{23} \end{bmatrix} \begin{pmatrix} u \\ z \\ p \end{pmatrix} + \begin{pmatrix} \zeta_1 \\ \zeta_2 \end{pmatrix} \tag{4.3}$$

for appropriate definitions of η_{ij}, ζ_i. To ensure that the new differential equation for z does not depend explicitly on p, we require that $\eta_{23} = 0$. Since calculations reveal

$$\eta_{23} = \frac{\gamma(\tau_1 - \tau_2)}{\tau_1 \tau_2 \, det A},$$

the new slow variable p will be decoupled from the resulting (u, w, z) system only if $\tau_1 = \tau_2$ (which is precisely how we defined the degenerate case).

By assuming $\tau_1 = \tau_2$, the choice

$$a_{11} = 1, \quad a_{12} = -\frac{\beta_1 \tau_2}{\beta_2 \tau_1}, \quad b_1 = \beta_1(\alpha_1 - \alpha_2) + 1 \tag{4.4}$$

then results in the transformed system

$$\frac{du}{dt} = f(u) - w - z, \tag{4.5}$$

$$\frac{dw}{dt} = g(u) - w, \tag{4.6}$$

$$\frac{dz}{dt} = \varepsilon \frac{H(u) - z}{\tau_1}, \tag{4.7}$$

$$\frac{dp}{dt} = \varepsilon \frac{1 - p}{\tau_1}, \tag{4.8}$$

where

$$H(u) = \beta^*(u - \alpha^*), \tag{4.9}$$

$$\beta^* = \beta_1 + \gamma\beta_2, \tag{4.10}$$

$$\alpha^* = \frac{\beta_1\alpha_1 + \gamma\beta_2\alpha_2}{\beta_1 + \gamma\beta_2}. \tag{4.11}$$

As claimed, we see that the variable p is decoupled from the rest of the system (4.5)–(4.7), showing the reduction of (FULL) to a one slow variable model (4.5)–(4.7). Furthermore, we see in (4.8) that as $t \to \infty$, $p \to 1$. In other words, $p = 1$ is a globally stable three-dimensional manifold on which the dynamics are determined by (4.5)–(4.7). Given (4.1) and (4.4), this implies that the projected trajectories of (FULL) are attracted to the line

$$y = \frac{\beta_2}{\beta_1}x + \beta_2(\alpha_1 - \alpha_2) \tag{4.12}$$

in the (x, y)-plane.

By comparing (4.7) to (2.9) and making the identification $(\beta, \alpha) = (\beta^*, \alpha^*)$, it is evident that on $p = 1$ there exist (β^*, α^*) with $\beta^* > 0$ such that (FULL) has bursting solutions. This assures us, in this degenerate case, that for some subset of slow parameter space there must exist a fixed point $\bar{x}$ for the return map $\phi(x)$.

We illustrate one such bursting solution and fixed point in Figure 4.1. There, XPPAUT [21] was used to numerically integrate (FULL) for the degenerate case $\lambda_s = (\beta_1, \beta_2, \alpha_1, \alpha_2, \tau_1, \tau_2) = (3, 0.5, -1, -3, 1, 1)$ with $\gamma = 0.7$. In Figure 4.1A we see square-wave bursting in the u versus t time trace for this run. In Figure 4.1B we see how the projected trajectory is attracted to the line $y = \frac{\beta_2}{\beta_1}x + \beta_2(\alpha_1 - \alpha_2)$, indicated as $p = 1$. Also superimposed in Figure 4.1B are the two curves Γ_- and Γ_{HC}. Lastly, we note that for this run, since $\beta_1 > 0$ and $\beta_2 > 0$, both x and y are activation variables. Given (4.10), it is clear that the signs of β_i need not be the same for β^* to be positive. Thus, in the degenerate case, combinations of activating and inactivating variables can result in bursting solutions.

4.1. Explicit construction of ϕ in the degenerate case. In this section we find an explicit formula for the map ϕ in the degenerate case. We do this by separately deriving $\widetilde{\phi}$ and $\widehat{\phi}$, after which a direct composition yields ϕ.

First, we determine the silent phase duration T_s. Differentiating (2.12) and using (4.7),

$$\frac{dz}{d\tau} = G'(u)\frac{du}{d\tau} = \frac{H(u) - G(u)}{\tau_1}.$$

Integrating this result,

$$\int_{u_{\text{HC}}}^{u_-} \frac{G'(u)}{H(u) - G(u)}\,du = \int_0^{T_s} \frac{1}{\tau_1}\,d\tau,$$

one may solve for

$$T_s = \tau_1 \int_{u_{\text{HC}}}^{u_-} \frac{G'(u)}{H(u) - G(u)}\,du. \tag{4.13}$$

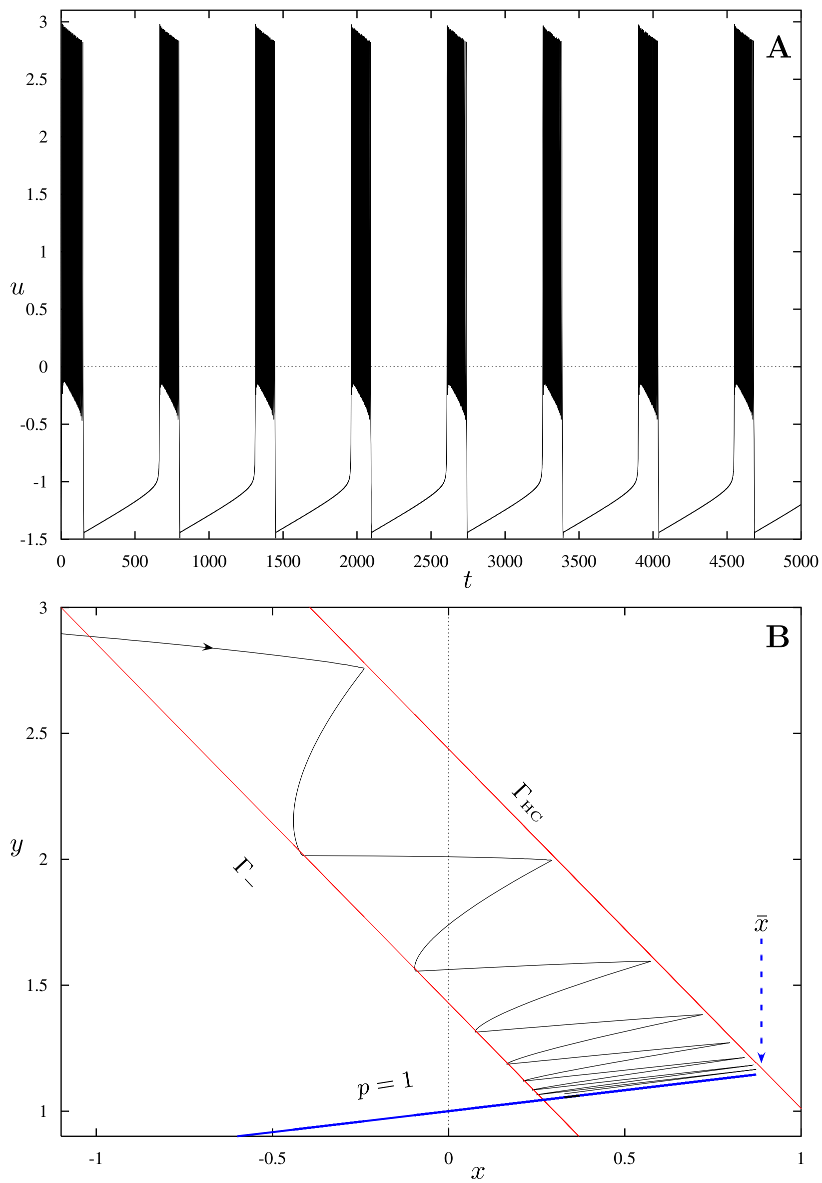

FIG. 4.1. *Illustration of the attraction of projected trajectories to $p = 1$ in the degenerate case.* **A** *shows u versus t for this run. In* **B** *we see the compression of trajectories projected into the (x, y)-plane to the line $y = \frac{\beta_2}{\beta_1}x + \beta_2(\alpha_1 - \alpha_2)$. Parameter values for the run are listed in the text.*

This is the time taken by a projected (SS) trajectory to traverse from $\mathbf{X}_n \in \Gamma_{\rm HC}$ to $\mathbf{X}_{n+1} \in \Gamma_-$, as illustrated in Figure 4.2. Also shown is the line $p = 1$, to which such trajectories are attracted, and the p coordinates p_n and p_{n+1} on $\Gamma_{\rm HC}$ and Γ_-, respectively.

Having found T_s, we integrate (4.8) in the slow time τ,

$$\int_{p_n}^{p_{n+1}} \frac{1}{1-p}\, dp = \int_0^{T_s} \frac{1}{\tau_1}\, d\tau,$$

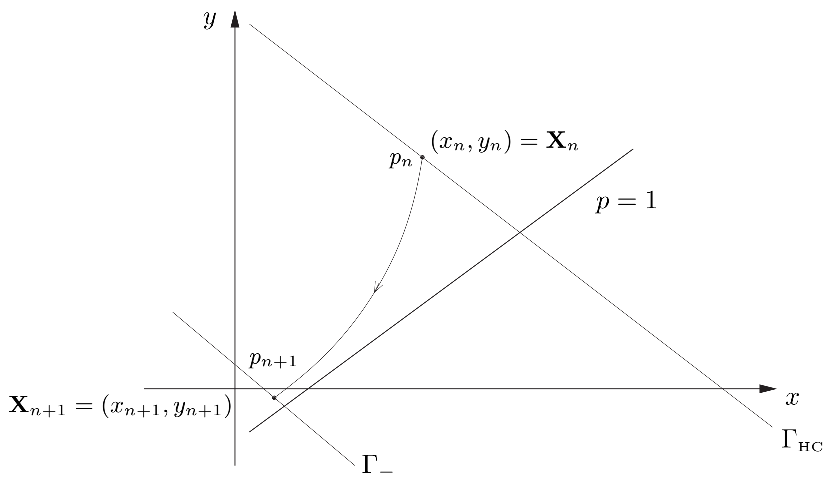

FIG. 4.2. *Projected trajectories on S_L associated with $\widetilde{\phi}$, the degenerate $\tau_1 = \tau_2$ case.*

and find that

$$\ln\left|\frac{1-p_n}{1-p_{n+1}}\right| = \frac{T_s}{\tau_1}. \tag{4.14}$$

However, (4.8) guarantees that $1 - p_n$ and $1 - p_{n+1}$ have the same sign, so we may drop the absolute values sign in (4.14) and solve for p_{n+1}:

$$p_{n+1} = 1 - (1 - p_n)\, e^{\frac{-T_s}{\tau_1}}. \tag{4.15}$$

To convert this expression back into our original (x, y)-coordinate system, we note that by using $\tau_1 = \tau_2$ and (4.4) in (4.1) one finds

$$p = \bar{P}(x, y) = x - \frac{\beta_1}{\beta_2} y + \beta_1(\alpha_1 - \alpha_2) + 1. \tag{4.16}$$

Thus, (4.15) becomes

$$\bar{P}\left(x_{n+1}, \frac{z_- - x_{n+1}}{\gamma}\right) = 1 - \left(1 - \bar{P}\left(x_n, \frac{z_{\mathrm{HC}} - x_n}{\gamma}\right)\right) e^{\frac{-T_s}{\tau_1}}, \tag{4.17}$$

which when solved for x_{n+1} allows us to finally obtain

$$x_{n+1} = \widetilde{\phi}(x_n) = e^{\frac{-T_s}{\tau_1}} x_n + b_s, \tag{4.18}$$

where

$$b_s = \bar{B}(T_s, z_-, z_{\mathrm{HC}}) \equiv \frac{\left(1 - e^{\frac{-T_s}{\tau_1}}\right)\beta_1\beta_2\gamma(\alpha_2 - \alpha_1) + \beta_1\left(z_- - z_{\mathrm{HC}} e^{\frac{-T_s}{\tau_1}}\right)}{\beta_1 + \gamma\beta_2}. \tag{4.19}$$

In a fashion analogous to the derivation of $\widetilde{\phi}$, we compute $\widehat{\phi}$ by integrating (4.8) over the active phase duration T_a. A leading-order value for T_a can be computed by integrating the averaged fast subsystem corresponding to the transformed system

(4.5)–(4.8). Applying the method of averaging to system (4.5)–(4.8), one finds its associated (AFS) is

$$\frac{dz}{d\tau} = \frac{\widehat{H}(z) - z}{\tau_1}, \tag{4.20}$$

$$\frac{dp}{d\tau} = \frac{1-p}{\tau_1}, \tag{4.21}$$

where

$$\widehat{H}(z) = H(\hat{u}(z)) = \beta^*(\hat{u}(z) - \alpha^*), \tag{4.22}$$

and $\hat{u}(z)$ is as defined in (2.21).

In order to compute the active phase duration T_a, we integrate (4.20) as follows:

$$\int_{z_-}^{z_{\mathrm{HC}}} \frac{dz}{\widehat{H}(z) - z} = \int_0^{T_a} \frac{1}{\tau_1}\, d\tau,$$

and then solve for T_a to find

$$T_a = \tau_1 \int_{z_-}^{z_{\mathrm{HC}}} \frac{dz}{\widehat{H}(z) - z}. \tag{4.23}$$

We let p_n be the p coordinate of an (AFS) trajectory with initial conditions $(x_n, y_n) \in \Gamma_-$. Similarly, we define p_{n+1} to be the p-coordinate of the (AFS) trajectory as it leaves the active phase at $(x_{n+1}, y_{n+1}) \in \Gamma_{\mathrm{HC}}$. Then, integrating (4.21),

$$\int_{p_n}^{p_{n+1}} \frac{1}{1-p}\, dp = \int_0^{T_a} \frac{1}{\tau_1}\, d\tau,$$

and proceeding exactly as we did in (4.14)–(4.17) while using the value of T_a from (4.23), we find

$$x_{n+1} = \widehat{\phi}(x_n) = e^{\frac{-T_a}{\tau_1}} x_n + b_a\,, \quad b_a = \bar{B}(T_a, z_{\mathrm{HC}}, z_-), \tag{4.24}$$

where the function $\bar{B}$ was defined in (4.19). Also, since $\phi(x) = \widehat{\phi}(\widetilde{\phi}(x))$, (4.18) and (4.24) imply

$$\phi(x) = e^{\frac{-(T_s+T_a)}{\tau_1}} x + b_{as}\,, \tag{4.25}$$

where $b_{as} = e^{\frac{-T_a}{\tau_1}} b_s + b_a$.

From this expression, the fixed point $\bar{x}$ of ϕ is easily computed as

$$\bar{x} = \frac{b_{as}}{1 - e^{\frac{-(T_s+T_a)}{\tau_1}}}. \tag{4.26}$$

It should be noted that the dependence of $\bar{x}$ on the active and silent durations in (4.26) is misleading. As can be seen in Figure 4.1, the fixed point can also be computed as that x value, where the line $p = 1$ intersects Γ_{HC}. Using (4.16), this value can be found by solving $\bar{P}(x, y) = 1$ and $x + \gamma y = z_{\mathrm{HC}}$ for x to find

$$\bar{x} = \frac{\gamma\beta_1\beta_2(\alpha_2 - \alpha_1) + \beta_1 z_{\mathrm{HC}}}{\beta_1 + \gamma\beta_2} = \frac{\gamma\beta_1\beta_2(\alpha_2 - \alpha_1) + \beta_1 z_{\mathrm{HC}}}{\beta^*}. \tag{4.27}$$

However, given the previous definitions, it is readily verified that (4.26) indeed simplifies to (4.27).

To conclude this section we make some observations about the dependence of the map ϕ on the (activation/inactivation) parameters β_1 and β_2. As was pointed out earlier, β_1 and β_2 need not be of the same sign for ϕ to have the fixed point calculated in (4.27). The issue here is, what degrees of activation and inactivation can lead to such degenerate bursting solutions? Since (4.8) has no dependence on these parameters, the answer to this question is equivalent to knowing the parameter sets (α^*, β^*) for which (4.5)–(4.7) has bursting solutions. A complete description of the set $\mathcal{B}$ of (α^*, β^*) pairs for which such bursting solutions exist is complex but well studied. For instance, for an appropriate $\beta^* > 0$, as α^* is varied the system makes a transition from bursting to continuous spiking via a complex sequence of bifurcations [54]. However, one can glean a few simple results from the explicit expressions for $\bar{x}$ and $\phi(x)$.

For example, when $\beta^* < 0$, system (4.5)–(4.7) typically does not have a bursting solution. Now suppose β^* is initially positive and $\beta_1 < 0$ (inactivation) is decreased while $\beta_2 > 0$ (activation) and $\alpha_k, k = 1, 2$ are held fixed. Given (4.10) and (4.27), one then sees that $\beta^* \to 0+$ and $|\bar{x}| \to \infty$. Alternately, as inactivation increases (with other parameters fixed), the fixed point of the map ϕ will increase in magnitude.

Lastly, we emphasize that other limiting cases may be possible since (α^*, β^*) depend on all $\beta_1, \beta_2, \alpha_1$, and α_2. However, from (4.25),

$$|\phi'(\bar{x})| = e^{\frac{-(T_s+T_a)}{\tau_1}} < 1$$

implies that no such limiting cases in the degenerate case can involve a destabilization of the fixed point $\bar{x}$. Moreover, the singular bursting solutions are always stable (in this degenerate case).

5. Numerically approximating ϕ in the nondegenerate case. In the nondegenerate case when $\tau_1 \neq \tau_2$, explicit formulas for $\widehat{\phi}$ and $\widetilde{\phi}$ remain elusive. In this section we outline a continuation technique for approximating these maps numerically. The technique requires recasting the map values as boundary conditions in two point boundary value problems which are homotopic to simpler problems whose solutions are known.

To be specific, the map $\widetilde{\phi}$ for the slow flow on $\mathbb{S}_L$ is computed as a solution of the following boundary value problem:

$$\frac{dx}{d\tau} = Tf_1(x, y, \lambda) = T\left(-(1-\lambda)x + \lambda F_1(x, y)\right), \tag{5.1}$$

$$\frac{dy}{d\tau} = Tf_2(x, y, \lambda) = T\left(-(1-\lambda)y + \lambda F_2(x, y)\right), \tag{5.2}$$

$$x(0) = x_0, \tag{5.3}$$

$$y(0) = (z_{\text{HC}} - x_0)/\gamma, \tag{5.4}$$

$$x(1) = x_f, \tag{5.5}$$

$$y(1) = (z_- - x_f)/\gamma, \tag{5.6}$$

where the vector field $\mathbf{F} = (F_1, F_2)$ is that of the (SS) in (2.18)–(2.19), T is a constant, λ is a homotopy parameter, and $\mathbf{f}(x, y, \lambda) \equiv (f_1, f_2)$. The boundary conditions (5.3)–(5.4) imply $(x(0), y(0)) \in \Gamma_{\text{HC}}$. Similarly, (5.5)–(5.6) imply $(x(1), y(1)) \in \Gamma_-$. Thus, solutions of this boundary value problem describe trajectories which start on Γ_{HC} and terminate on Γ_-. When $\lambda = 1$, $\mathbf{f}(x, y, 1) = \mathbf{F}(x, y)$, so that $x_f = \widetilde{\phi}(x_0)$ providing

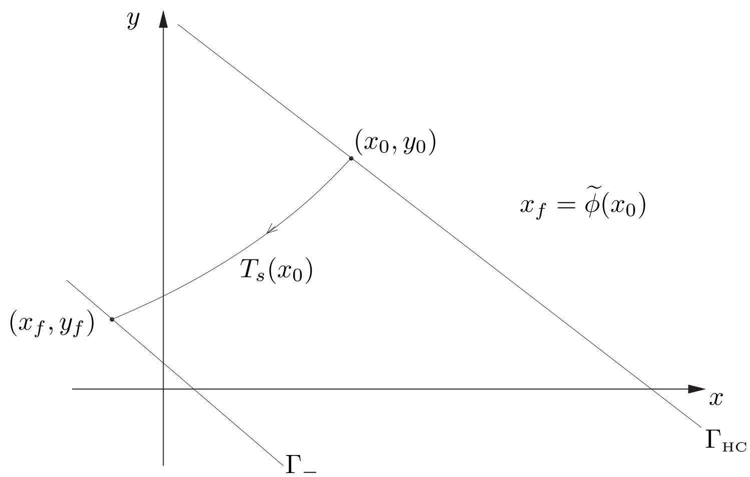

FIG. 5.1. *An illustration of $\widetilde{\phi}$ and the (SS) projected into the (x, y)-plane.*

$T = T_s$, the silent phase duration. A diagram illustrating this $\lambda = 1$ case is shown in Figure 5.1.

When $\lambda = 0$, the solution of (5.1)–(5.6) is known explicitly:

$$x(\tau) = x_0 e^{-\tau T}, \quad y(\tau) = \frac{z_{\text{HC}} - x_0}{\gamma} e^{-\tau T}, \quad T = ln\left(\frac{z_{\text{HC}}}{z_-}\right), \quad x_f = x_0 e^{-T}.$$

AUTO [19, 20] was then used to numerically continue this known solution to the $\lambda = 1$ case while letting the three parameters (λ, x_f, T) vary. Then, keeping $\lambda = 1$ fixed, (x_0, x_f, T) are allowed to vary in a subsequent run over a prescribed range of initial x values x_0. Given Figure 5.1, the resulting x_f values are $\widetilde{\phi}(x_0)$, and T is the silent phase duration T_s.

Results of these calculations are illustrated in Figures 5.2(a) and 5.2(b). There, $\widetilde{\phi}(x)$ is illustrated for the two-parameter sets listed in Table 5.1. For the $(+,+)$ case (Figures 5.2(a), (c), (e)) where $\beta_i > 0$, both x and y model activating variables in (FULL). In an analogous fashion, the $(+,-)$ case (Figures 5.2(b), (d), (f)) models the competing effect of activating and inactivating variables. Superimposed on the figures is the line $y = x$ as a point of reference. As a note, however, the fixed points of $\widetilde{\phi}(x)$ do not correspond to bursting solutions of (FULL).

The technique for generating $\widehat{\phi}$ from the (AFS) is similar. One first defines the boundary value problem

$$\frac{dx}{d\tau} = Tg_1(x, y, \lambda) = T\left(x(1-\lambda) + \lambda \widehat{G}_1(x, y)\right), \tag{5.7}$$

$$\frac{dy}{d\tau} = Tg_2(x, y, \lambda) = T\left(\lambda \widehat{G}_2(x, y)\right), \tag{5.8}$$

$$x(0) = x_0, \tag{5.9}$$

$$y(0) = (z_- - x_0)/\gamma, \tag{5.10}$$

$$x(1) = x_f, \tag{5.11}$$

$$y(1) = (z_{\text{HC}} - x_f)/\gamma, \tag{5.12}$$

TABLE 5.1
Standard parameter sets.

	β_1	α_1	β_2	α_2	γ	τ_1	τ_2
$(+,+)$	3	-1	0.5	-3	0.7	0.9	1
$(+,-)$	4	-1	-1	-0.7	1	1	0.3

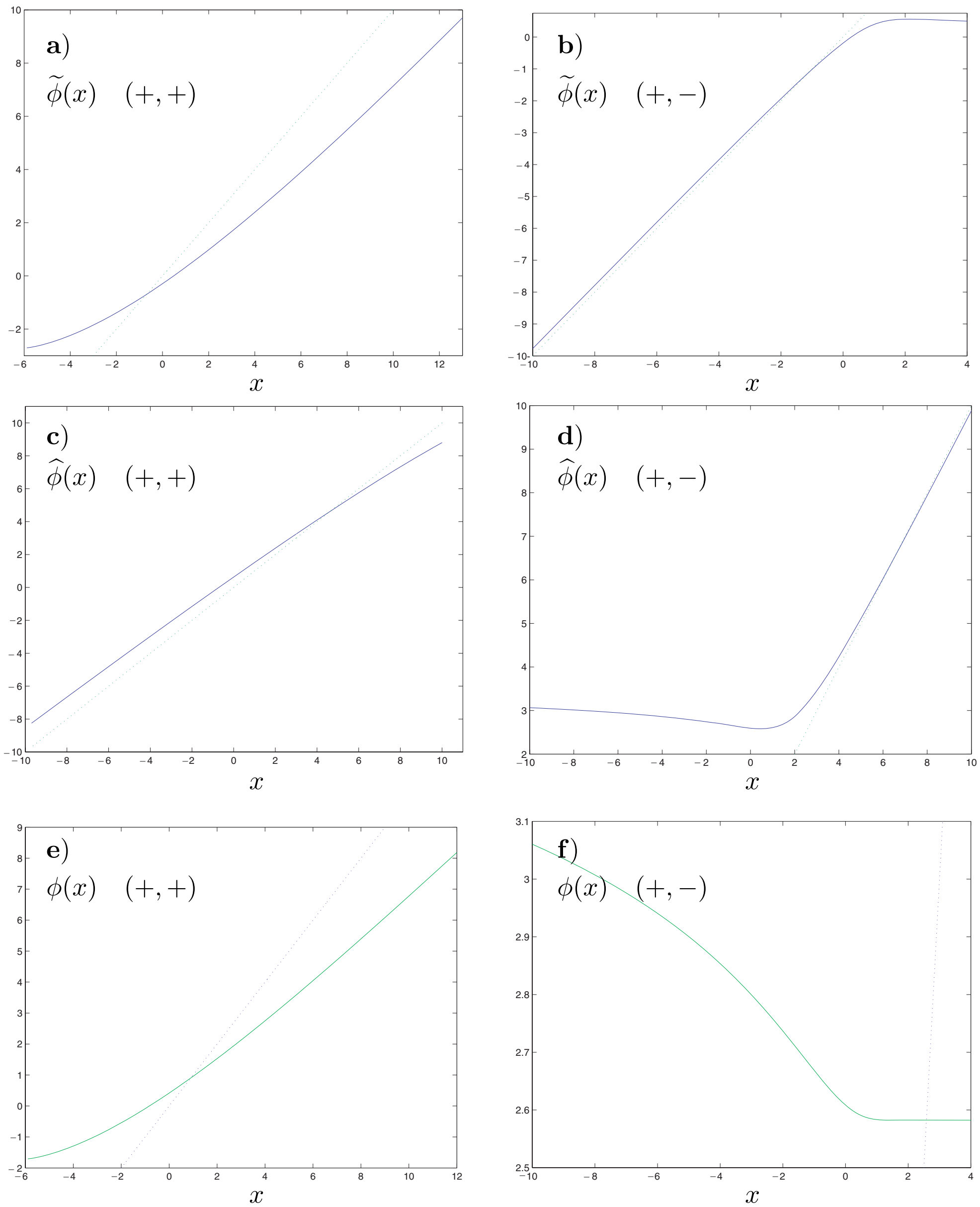

FIG. 5.2. *Maps $\widetilde{\phi}$, $\widehat{\phi}$, and $\phi(x)$ generated numerically using AUTO. Shown are $\widetilde{\phi}(x)$, $\widehat{\phi}(x)$, and $\phi(x)$ for a range of initial x values; the $(+,+)$ case is shown in* **a**, **c**, **e**; *the $(+,-)$ case in* **b**, **d**, **f**. *Parameter values for each computation are tabulated in Table* 5.1.

where the vector field $\widehat{\mathbf{G}} = (\widehat{G}_1, \widehat{G}_2)$ is that defined in (2.22)–(2.23), and $\mathbf{g}(x, y, \lambda) \equiv (g_1, g_2)$. As before, $\mathbf{g}(x, y, 1) = \widehat{\mathbf{G}}(x, y)$ implies $x_f = \widehat{\phi}(x_0)$ when T is the active phase duration T_a.

However, the problem (5.7)–(5.12) differs from (5.1)–(5.6) in an essential way. In the former, the vector field $\mathbf{g}(x, y, 0) = (x, 0)$ was chosen to match the flow direction of the (AFS) *from* Γ_- to Γ_{HC}. In contrast, the flow direction of $\mathbf{f}(x, y, 0) = (-x, -y)$ was chosen so that trajectories starting on Γ_{HC} would terminate on Γ_-. The choice of initial ($\lambda = 0$) vector fields is not unique. Here we have chosen simple ones which retain the flow directionality of each subsystem and whose analytic solution is known. For the choice $\mathbf{g}(x, y, 0) = (x, 0)$, the exact initial solution is

$$x(\tau) = x_0 e^{\tau T}, \quad y(\tau) = \frac{z_- - x_0}{\gamma}, \quad T = ln\left(\frac{z_{\mathrm{HC}} - z_- + x_0}{x_0}\right), \quad x_f = x_0 e^T.$$

In an analogous fashion, AUTO was used to continue this solution in λ and then in x_0 to generate the map $x_f = \widehat{\phi}(x_0)$. In all these runs the approximation (2.24) of $\hat{u}(z)$ was used.

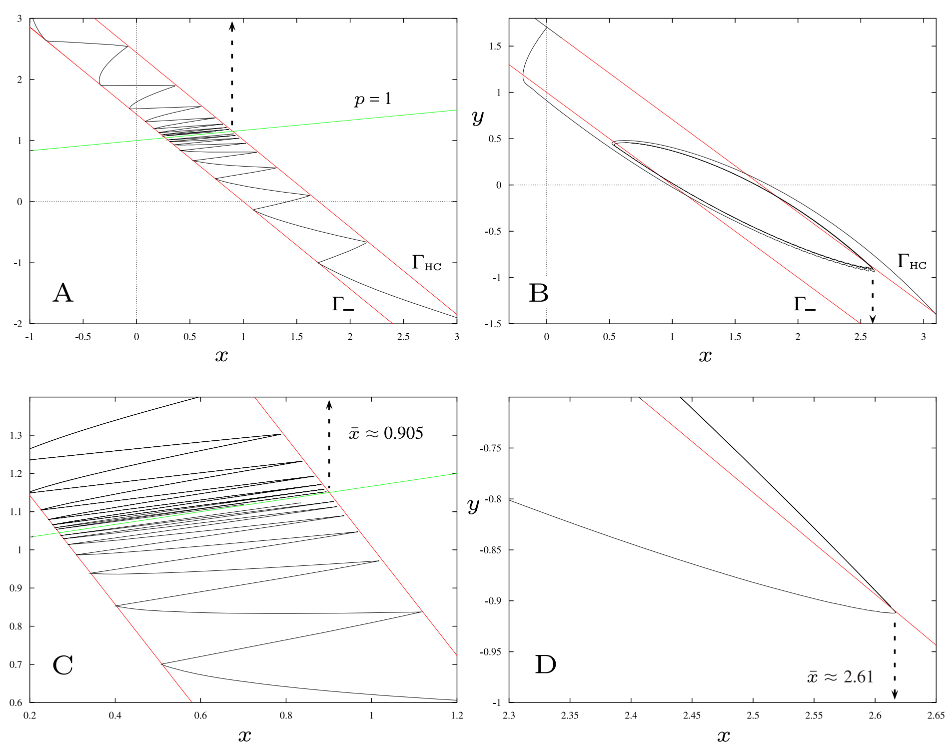

FIG. 5.3. *Verification of the fixed point $\bar{x} = \phi(\bar{x})$ obtained in the map composition illustrated in Figure 5.2. The two figures on the left are the $(+,+)$ case and the two on the right are the $(+,-)$ case. In* **A** *we see the projection of two trajectories of (FULL) into the (x, y)-plane appearing to compress toward the superimposed line $p = 1$. In* **C** *we have enlarged the region of interest about the map fixed point $\bar{x} \approx 0.905$. Also shown in* **A** *and* **C** *are the curves Γ_- and Γ_{HC}. In* **B** *we also see the projection of two trajectories of (FULL) into the (x, y)-plane, but in the $(+,-)$ case. The two projected trajectories wind onto a cycle in the (x, y)-plane. In* **D** *we are able to discern the map fixed point of $\bar{x} \approx 2.61$.*

Results of the calculations for $\widehat{\phi}$ and the respective compositions $\underset{\sim}{\phi} = \widehat{\phi} \circ \widetilde{\phi}$ are shown in Figure 5.2 for the same parameter values used to compute $\underset{\sim}{\phi}$. The latter compositions were computed by numerically composing the data which generated $\widehat{\phi}$ and $\widetilde{\phi}$. Superimposed on the graphs of $\phi(x)$ is the line $y = x$ to indicate the location of the fixed point $\bar{x}$ corresponding to bursting solutions of (FULL). The interpolated values of the fixed points found in this manner were $\bar{x} \approx 0.905$ and $\bar{x} \approx 2.58$ for the $(+,+)$ and $(+,-)$ cases, respectively.

To separately verify these fixed point values, (FULL) was numerically integrated in Figure 5.3 over many silent and active phase cycles for the parameter values in Table 5.1. As can be seen, the projections of these solutions ultimately approach a periodic orbit, and the fixed point values computed from these figures closely agree with those computed from Figure 5.2. In all, these numerical results suggest that singular bursting solutions persist for nondegenerate parameter values. In the (+,+) case shown in Figure 5.3A, the parameter set is "nearly" degenerate and the projected bursting solution lies near the line $p = 1$. In contrast, the bursting cycle in the $(+,-)$ (activation/inactivation) case does not lie near the $p = 1$ line. In fact, the projected active and silent phase trajectories of that $(+,-)$ case are nearly tangent to the transition curves Γ_{HC} and Γ_{-}. From this observation, one might conjecture that bursting solutions do not persist for all parameter values. For example, the presence of a strongly attractive equilibria of (FULL) on $\mathbb{S}_L$ might significantly alter the (SS) flow to the point that trajectories may not be attracted to a bursting solution. These issues are explored in the next section.

6. A bistable case. In this section we demonstrate numerically that system (FULL) can exhibit bistability between bursting solutions and equilibria on $\mathbb{S}_L$. Just such an example is illustrated in Figure 6.1. Slow parameters λ_s were chosen so that (FULL) had a stable fixed point $\mathbf{X}_e$ on the lower branch $\mathbb{S}_L$ (see [25] for a detailed treatment of how to determine equilibria location and stability dependence on λ_s). In Figure 6.1B the u component of a bursting solution resulting from a particular set of initial conditions is shown. The projection of this solution onto the xy-plane is shown in Figure 6.1A. However, by choosing initial conditions near $\mathbb{S}_L$ in the basin of attraction of $\mathbf{X}_e$, the solution of (FULL) is shown to approach $\mathbf{X}_e$ in Figures 6.1C, D. The projection of the bursting solution in Figure 6.1A is also shown in Figure 6.1C for comparison.

For the bistability demonstrated in Figure 6.1 to occur, a few things must happen simultaneously. Minimally, (FULL) must have a stable equilibrium $\mathbf{X}_e$ on $\mathcal{S}_L$. However, even if parameters are chosen so that $\mathbf{X}_e \in \mathcal{S}_L$, it is not immediately clear if $\mathbf{X}_e$ will be stable or if the map ϕ can simultaneously have a stable fixed point. In this section, we shall give a brief synopsis of some issues regarding these points. First, we address issues concerning equilibria stability and location. Later, we determine some necessary conditions that map domains and ranges must satisfy for this type of bistability to occur.

The equilibria $\mathbf{X}_e$ of (FULL) have coordinates $\mathbf{X}_e = (\bar{u}, \bar{w}, \bar{x}, \bar{y})$ where, given (2.8), $\bar{u}$ are roots of

$$\Delta(u) = -G(u) + h_1(u) + \gamma h_2(u) = u^3 + au + b, \tag{6.1}$$

where

$$a = \beta_1 + \gamma\beta_2 - 3, \tag{6.2}$$

$$b = -(\alpha_1\beta_1 + \gamma\alpha_2\beta_2 + 3), \tag{6.3}$$

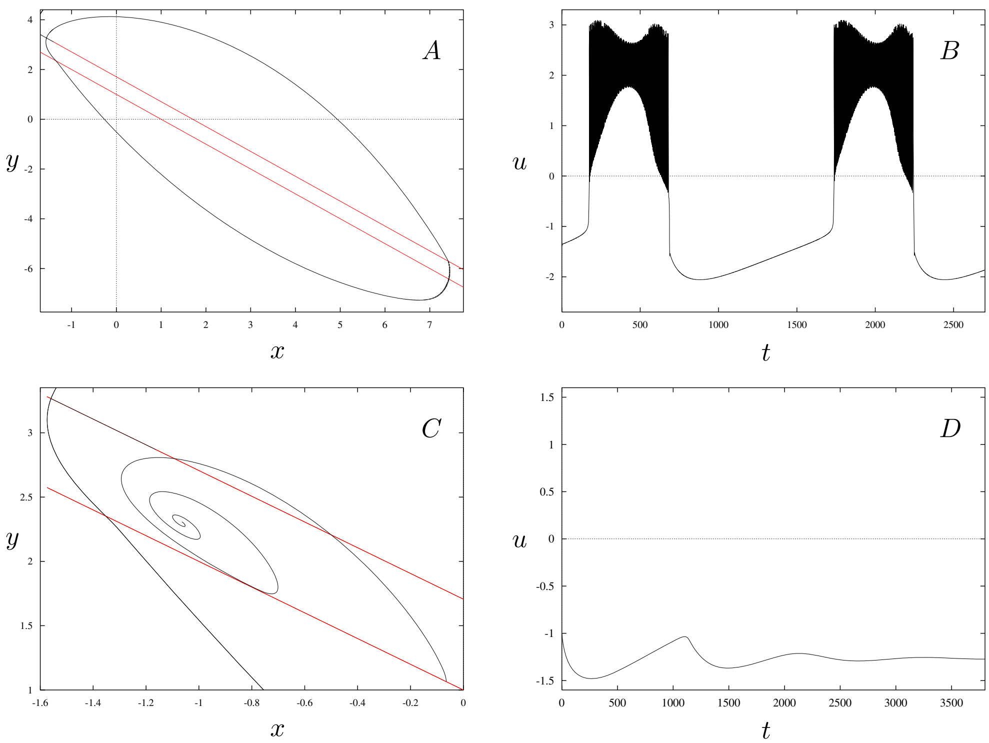

FIG. 6.1. *Numerical illustration of bistability. In both simulations the slow parameters were* $\lambda_s = (\beta_1, \beta_2, \alpha_1, \alpha_2, \tau_1, \tau_2) = (4, -3, -1, -0.5, 1, 0.3)$. *A and C are projections of the solutions of (FULL) for different initial conditions. B and D show the corresponding* $u(t)$ *component in each simulation.*

and $\bar{w} = g(\bar{u})$, $\bar{x} = h_1(\bar{u})$, and $\bar{y} = h_2(\bar{u})$. From this we note that $\mathbf{X}_e \in \mathcal{S}_L$ only if (a, b) is an element of the parameter space:

$$D_L = \{(a, b) : b = -ua - u^3, u < u_- = -1\}.$$

Thus, D_L can be characterized as the union of all those lines in the (a, b)-plane having slope $-u$ and that intercept $-u^3$ with $u < u_-$. We note, however, that even if the slow parameters λ_s are chosen so that $(a, b) \in D_L$, (FULL) may have other equilibria (see [25] for a detailed treatment of how to determine equilibria numbers and locations). Moreover, if equilibria occur on the upper branch ($u > u_+$) near the limit cycles of the (FS), it is possible that the (AFS) itself can have a fixed point. With the dynamics of the (AFS) changed, bursting solutions may no longer be possible. Thus, when searching a parameter space for the type of bistability described in this section, it is reasonable to restrict oneself to seeking parameters for which (FULL) has a unique equilibrium on $\mathcal{S}_L$. Given the cubic form of $\Delta(u)$, (FULL) will have a *unique* equilibrium $\mathbf{X}_e \in \mathcal{S}_L$ if and only if $(a, b) \in D_L$ and the discriminant

$$D_\Delta = \frac{b^2}{4} + \frac{a^3}{27} > 0. \tag{6.4}$$

Next, we address the stability of the (unique) equilibrium $\mathbf{X}_e \in \mathcal{S}_L$. Toward this end, we define $P(\lambda)$ as the characteristic polynomial of the Jacobian $D\vec{\mathbf{F}}(\mathbf{X}_e)$ of

(FULL) at $\mathbf{X}_e$ with roots λ of P being the eigenvalues. Similarly, we define $P_0(\lambda)$ as the characteristic polynomial of the Jacobian of the (FS). Using these definitions and the expansion

$$\lambda = \lambda_0 + \varepsilon\lambda_1 + \varepsilon^2\lambda_2 + \cdots$$

in $P(\lambda)$, one finds

$$P(\lambda) = \lambda_0^2 P_0(\lambda_0) + \varepsilon P_1(\lambda_0, \lambda_1) + \varepsilon^2 P_2(\lambda_0, \lambda_1, \lambda_2) + O(\varepsilon^3), \tag{6.5}$$

where for the moment we do not explicitly state the functions P_0, P_1, P_2. Since (FULL) has two fast variables and two slow variables, two of the eigenvalues $\lambda = O(1)$, while the remaining two eigenvalues $\lambda = O(\varepsilon)$. For $\mathbf{X}_e$ to be stable we require all four eigenvalues to have $\Re e(\lambda) < 0$. Clearly, if $\mathbf{X}_e \in \mathcal{S}_L$, the two $O(1)$ eigenvalues have $\Re e(\lambda) < 0$ since such λ's equal λ_0 to leading order and the roots $\lambda_0 \neq 0$ of P_0 are the same eigenvalues as in the (FS). Thus, it suffices to examine the $O(\varepsilon)$ eigenvalues, whose expansions have $\lambda_0 = 0$.

For the $\lambda_0 = 0$ case, it is easily verified that

$$P_1(0, \lambda_1) = 0 \qquad \forall \lambda_1.$$

So the "small" $O(\varepsilon)$ eigenvalues associated with the (SS) require examining the $O(\varepsilon^2)$ term in (6.5). Explicit calculations reveal

$$P_2(0, \lambda_1, \lambda_2) = Q(\lambda_1) \equiv q_2\lambda_1^2 + q_1\lambda_1 + q_0, \tag{6.6}$$

where the coefficients of Q in (6.6) are given by

$$q_2 = -G'(\bar{u}), \tag{6.7}$$

$$q_1 = \frac{\beta_1\tau_2 + \gamma\beta_2\tau_1 - G'(\bar{u})(\tau_1 + \tau_2)}{\tau_1\tau_2}, \tag{6.8}$$

$$q_0 = \frac{\beta_1 + \gamma\beta_2 - G'(\bar{u})}{\tau_1\tau_2}. \tag{6.9}$$

Notice that there is no dependence on λ_2 in $P_2(0, \lambda_1, \lambda_2)$, and that Q is quadratic in λ_1. Also, for the remainder of this section we drop the overbar notation on u.

The leading term λ_1 of these small eigenvalues is determined as the roots of Q in (6.6):

$$\lambda_1^{\pm} = \frac{-q_1 \pm \sqrt{q_1^2 - 4q_2q_0}}{2q_2}. \tag{6.10}$$

Since $u < u_- = -1$ on $\mathcal{S}_L$, the quantity $G'(u) = -3u^2 + 3$ is negative on $\mathcal{S}_L$ and

$$\mathbf{X}_e \in \mathcal{S}_L \Rightarrow q_2 > 0. \tag{6.11}$$

This result and the signs of the coefficients (q_1, q_0), based on the signs of the activation parameters[3] (β_1, β_2), are organized in Table 6.1 and are discussed in the following text. Given the signs of the coefficients q_i, we are then able to determine the stability of $\mathcal{S}_L$ equilibria. Throughout, recall $0 < \gamma$, $0 < \tau_i$, $i = 1, 2$, and (6.11), i.e., $q_2 > 0$.

[3]Recall that x is a slow activation variable if $\beta_1 > 0$ and is a slow inactivation variable if $\beta_1 < 0$. Analogous remarks hold for y and β_2.

TABLE 6.1
Stability dependence of the equilibria $\mathbf{X}_e \in \mathcal{S}_L$ on the activation/inactivation parameters (β_1, β_2), where (q_2, q_1, q_0) are the coefficients of the quadratic $Q(\lambda)$ defined in (6.6). In the "Case" column, $(+,-)$ indicates the respective signs of β_1 and β_2. In the other columns, $+/-$ indicates that both signs of the column quantity are possible. In both the $(+,-)$ and $(-,+)$ cases, the equilibria $\mathbf{X}_e$ can undergo a Hopf bifurcation, and thus may be stable or unstable.

Case	sign(q_2)	sign(q_1)	sign(q_0)	Equilibria $\mathbf{X}_e$
$(+,+)$	$+$	$+$	$+$	stable
$(-,-)$	$+$	$+$	$+$	stable
		$+/-$	$-$	saddle
$(+,-)$	$+$	$+/-$	$+/-$	Hopf bifurcation possible
$(-,+)$	$+$	$+/-$	$+/-$	Hopf bifurcation possible

When $(\beta_1, \beta_2) = (+,+)$, i.e., both are positive, one sees immediately that $q_1 > 0$ and $q_0 > 0$ as well. As such, any $\mathcal{S}_L$ equilibria in this case will be stable, as noted in Table 6.1.

When $(\beta_1, \beta_2) = (-,-)$, it is possible for q_0 to be positive or negative. To understand this case we first note from (6.1) that

$$\Delta'(u) = -G'(u) + (\beta_1 + \gamma\beta_2). \tag{6.12}$$

If $q_0 > 0$, then $G'(u) < \beta_1 + \gamma\beta_2$, and we may conclude $\Delta'(u) > 0$. Rewriting q_1 in terms of $\Delta(u)$, we find

$$q_1 = \frac{\Delta'(u)}{\tau_1} + \frac{\Delta'(u)}{\tau_2} - \frac{\gamma\beta_2}{\tau_1} - \frac{\beta_1}{\tau_2}. \tag{6.13}$$

We now see that if $(\beta_1, \beta_2) = (-,-)$ and $q_0 > 0$, then $q_1 > 0$ so that $\mathbf{X}_e \in \mathcal{S}_L$ are stable.

If $(\beta_1, \beta_2) = (-,-)$ and $q_0 < 0$, then q_1 may be positive or negative. Moreover, in this case, $\sqrt{q_1^2 - 4q_2q_0} > |q_1|$ so that $\lambda_1^{\pm}$ are both real and have opposite signs. Then, $\mathbf{X}_e$ has a one-dimensional unstable manifold and a three-dimensional stable manifold. We list such unstable equilibria $\mathbf{X}_e$ of (FULL) in Table 6.1 as "saddles" since the associated equilibria $(\bar{x}, \bar{y})$ of the (SS) will be saddles.

Finally, we consider the $(\beta_1, \beta_2) = (+,-)$ and $(\beta_1, \beta_2) = (-,+)$ cases together. It is not hard to see in that restrictions on the sign of q_0 do not place similar restrictions on the sign of q_1; any sign is possible. Thus, $\lambda_1^{\pm}$ may be complex conjugate pairs, and transverse crossings of the imaginary axis could be possible. We do not discuss the details of this here but merely note that $\mathbf{X}_e$ may be stable or unstable and that Hopf bifurcations of such equilibria are possible (see [25] for a detailed treatment).

At this stage we summarize some of the previous results. First, to ensure there is a unique equilibria $\mathbf{X}_e \in \mathcal{S}_L$, slow parameters must be chosen so that $(a, b) \in D_L$ while simultaneously satisfying (6.4). The stability of such equilibria will largely depend on the sign of the activation/inactivation parameters (β_1, β_2). This dependence is summarized in Table 6.1. In Figure 6.1, the slow parameters were chosen to satisfy these conditions in the $(\beta_1, \beta_2) = (+,-)$ case. Moreover, in this case $\lambda_1^{\pm}$ were complex conjugates to create the spiral motion depicted in Figure 6.1C. We do not exclude the possibility of bistability for the other cases in Table 6.1. Even if this issue is resolved, it does not address issues concerning the simultaneous coexistence of a stable fixed point of the map ϕ needed to ensure the existence of a stable bursting solution. To address this latter issue, we examine the map domains and ranges defined in previous sections.

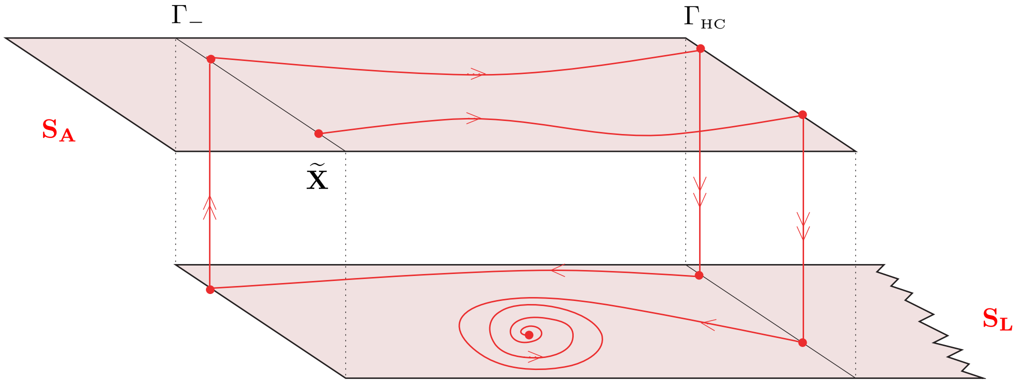

FIG. 6.2. *Illustration of bistability between bursting solutions and stable equilibria of (FULL). One solution illustrated has an initial condition $\widetilde{\mathbf{X}} \in S_A$ in the active phase but with $\hat{\Phi}(\widetilde{\mathbf{X}})$ in the basin of attraction of an equilibria of (FULL) on S_L. Also shown is a bursting cycle associated with the fixed point of Φ.*

First, we note that Figure 6.2 illustrates the simulations shown in Figure 6.1. In the following discussion we assume the domain $D(\widehat{\phi}) = \mathbb{R}$, whereas $D(\widetilde{\phi})$ is a proper subset of $\mathbb{R}$. While shortly it will become evident that the latter is necessary for bistability, we acknowledge that the former assumption is not. For example, for other parameter values the (AFS) may itself have a stable fixed point. For simplicity, we assume this is not the case in the following discussion.

For the system to exhibit the bistability illustrated in Figure 6.2, some trajectories of the (SS) originating along Γ_{HC} must be attracted to the equilibria $\mathbf{X}_e$ on $\mathbb{S}_L$. Since $D(\widetilde{\phi})$ consists only of initial x-coordinates for which the (SS) trajectories starting on Γ_{HC} reach Γ_-, we conclude that in the bistable case, $D(\widetilde{\phi})$ must be a proper subset of $\mathbb{R}$.

Now, consider an initial condition where $\widetilde{\mathbf{X}} = (x_0, y_0) \in \Gamma_-$ and the fast variables are sufficiently near the (FS) limit cycle $\Omega(t, z_0), z_0 = x_0 + \gamma y_0$. To leading order, the resulting trajectory $\gamma_{\widetilde{X}}$ will traverse the active phase as described by the (AFS). Since $x_0 \in D(\widehat{\phi})$, $\gamma_{\widetilde{X}}$ will eventually reach Γ_{HC} and exit to the silent phase. Such a trajectory will enter the silent phase at an x-coordinate $\widehat{\phi}(x_0) \in R(\widehat{\phi})$.[4] The next issue is whether $\widehat{\phi}(x_0) \in D(\widetilde{\phi})$. If $\widehat{\phi}(x_0) \in D(\widetilde{\phi})$, then the trajectory starting in the active phase will eventually traverse the entire slow manifold and make a transition back to the active phase. The set of x values on the slow manifold for which this is possible is the previously discussed set $W = R(\widehat{\phi}) \cap D(\widetilde{\phi})$. Since $D(\widetilde{\phi})$ must be a proper subset of $\mathbb{R}$ in the bistable case, it follows that W must also necessarily be a proper subset of $\mathbb{R}$. The next issue is whether W is equal to or is a proper subset of $D(\widetilde{\phi})$. Clearly, $W \neq D(\widetilde{\phi})$; if it were, no (AFS) trajectory making a transition into the silent phase would ever be in the basin of attraction of the equilibria $\mathbf{X}_e$ on $\mathbb{S}_L$, and bistability would not be possible. To summarize, two necessary conditions for the system to exhibit bistability are

$$D(\widetilde{\phi}) \subset \mathbb{R}, \quad W = R(\widehat{\phi}) \cap D(\widetilde{\phi}) \subset D(\widetilde{\phi}),$$

with the understanding that the inclusions are proper.

[4]The range $R(\widehat{\phi})$ of $\widehat{\phi}$.

To conclude this section we remark that the above conditions, though necessary, may not be sufficient for bistability. For example, even if $\widehat{\phi}(x_0) \in D(\widetilde{\phi})$, in the next iterate it may be that $(\widehat{\phi} \circ \widetilde{\phi} \circ \widehat{\phi})(x_0) \notin D(\widetilde{\phi})$—in which case the trajectory would eventually be attracted to the equilibria $\mathbf{X}_e$. To completely resolve these types of details, accurate estimations of the map domains and ranges are paramount. We do not make such estimates in this paper, but some progress toward resolving these issues is presented in [25].

7. Conclusion and discussion. In this paper we have shown how singular approximations of bursting solutions of a model with two slow variables can be identified with fixed points of a one-dimensional map. When the time constants of the slow variables are equal (the degenerate case), the map and fixed point can be computed explicitly. Such a calculation is possible because, in that case, the system decouples under a simple transformation. Furthermore, from the transformed system (4.5)–(4.8) it was deduced that the original model has singular bursting solutions even if the slow variables are activating ($\beta_1 > 0$) and inactivating ($\beta_2 < 0$). In other studies both slow variables were inhibitory [51]. It was also shown that as inactivation was increased in this degenerate case, the magnitude of the fixed point $\bar{x}$ increased. Further, given the negative slope of the curve Γ_{HC}, as $\bar{x}$ increases the associated $\bar{y}$ value decreases. Insofar as the model studied in this paper is homotopic to other two slow variable models exhibiting bursting, the $(\bar{x}, \bar{y})$ would represent the extreme values of the slow regulatory variables (i.e., calcium concentration, channel activation variable) at the start of the silent phase. Thus, experimentally, if the slow regulatory variables have similar time constants, one might expect to see these extreme values increase and decrease inversely as inactivation of one process is increased. However, independent of the levels of activation and inactivation, no bifurcations of the bursting solution through a destabilization of the map fixed point are possible in the degenerate case. Moreover, as previously noted, the singular bursting solutions are always stable in this degenerate case.

In the more generic nondegenerate case when the time constants of the slow variables are not equal, it was demonstrated in section 5 how the maps used to determine bursting solutions can be computed by solving two one-parameter families of boundary value problems. There, AUTO [19] was used to homotope from known solutions to a solution which describes trajectories of the (SS) and the (AFS) of the original model. The methods described in section 5 would be substantially faster than using multiple integrations of (FULL) to compute the Poincaré return maps. Moreover, since AUTO automatically detects a variety of bifurcations, the aforementioned methods would be far better suited for numerical studies of bifurcations of bursting solutions in systems with two slow variables.

Some of the numerical techniques presented in section 5 might be adaptable to other models of bursting. For instance, in other models, slow subsystems can often be computed explicitly so that system (5.1)–(5.2) can be coded. However, in models such as (1.1)–(1.2), saddle-node and homoclinic bifurcation points of the associated fast subsystems are not known explicitly. Thus, it may not be possible to explicitly code boundary conditions such as (5.4) and (5.6). One possible resolution to this difficulty is to augment (5.1)–(5.6) with the (FS) of the model. It should be noted that similar issues would arise when attempting to code (5.7)–(5.12) in other models. In addition to the aformentioned issues, the vector field of the (AFS) of other models is not explicitly known. However, this issue can be circumvented by first calculating averaged quantities over a grid of slow variable values. Then, intermediate values can be computed using interpolation from this tabulated data within the AUTO code. In [25] such a method was implemented to determine $\hat{\phi}$ for the model defined in this paper.

Of additional importance is the bistability between bursting solutions and equilibria of (FULL) demonstrated in section 6. This is a fundamentally new type of bistability. In two variable neuron models, such as the FitzHugh–Nagumo model [23, 35], one variable is often slow and the other fast. The resulting (FS) exhibits bistability between equilibria. Bistability in the (FS) of three variable models exhibiting bursting is typically between stable equilibria and planar limit cycles. Such is the case in the (FS) of the model studied here. Even this type of bistability should be contrasted with bistability between stable periodic solutions such as that studied by Canavier et al. [10, 11]. Shilnikov, Calabrese, and Cymbalyuk [47] have also examined bistability between bursting solutions and (tonic) periodic solutions in a neuronal model with one slow variable. In this study, the bistability discussed in section 6 is between equilibria and (four-dimensional) bursting solutions. Regarding (FULL) as a model of neural activity, this type of bistability suggests some interesting potential neural dynamics. For instance, certain perturbations could switch the neural activity between bursting modes and quiescent modes. Since bursting typically acts on a time scale an order of magnitude larger than tonic spiking, this might have functional relevance in regulating physiological processes on time scales of the order of many bursts.

The former type of bistability is also of interest as it relates to the issue of why some isolated pancreatic β-cells burst while others do not [50]. Bursting electrical activity is observed in β-cells that are still intact in the islets [42]. At elevated temperatures (e.g., 30° C), bursting is also observed in β-cells that are isolated from the islets [48]. Yet, in other experiments at room temperature, isolated β-cells exhibit irregular spiking but do not burst [22]. Some researchers have discussed how the fundamental stochasticity of the β-cells might explain these different behaviors [42]. In other studies [37, 38], cell heterogeneity and diffusive coupling was a premise used to explain this experimental fact. There it was shown that if collections of cells with a stable equilibria were diffusively coupled to collections of bursting cells, the coupled system could burst synchronously. However, this explanation used a model with a sole slow variable. Since most recent models of β-cell electrical activity have two or more slow variables, it now appears that cell bistability might also play a role. For instance, if for some parameter sets these newer models exhibit the same sort of bistability demonstrated in section 6, then the experimental preparation could play a role. Some extracted cells may not burst merely because those preparations have slow variable values in the basin of attraction of the stable equilibria on S_L. Moreover, if the latter basin of attraction were sufficiently large, then even noise would not affect the result. Alternately, the sporadic spiking of "nonbursters" might be due to the noise (or channel stochasticity) being sufficiently large so that the (SS) trajectories traverse close to the basin of attraction of the equilibria $\mathbf{X_e}$. When properly exploring such ideas using a model, the size of the map domains become especially important. Also, in this case, the analytical and numerical tools developed in this paper may be particularly useful.

We note, however, that it is not known if the more recent β-cell models can exhibit such bistability for other parameter values. Additionally, we currently have no systematic way of determining such parameter sets. For the model used in this paper, some advances in solving this latter problem are presented in [25]. Although it is not too difficult to determine parameter sets where (FULL) has stable equilibria on S_L, it is difficult to determine a subset of such a parameter space where the model simultaneously exhibits bursting. As mentioned previously, the latter is intimately connected with domain issues of the maps $\tilde{\phi}$ and $\hat{\phi}$, which requires knowledge of certain global information about the slow and averaged fast subsystems.

The bistability discussed in section 6 also presents some other interesting modeling possibilities. For instance, if collections of such cells are coupled, then aggregate behavior would depend greatly on initial conditions. In reaction diffusion systems where bistability is between equilibria, traveling wave phenomena are ubiquitous. If the bistability is between equilibria and bursting solutions, the question arises if wavefronts separating such behaviors are possible. Even if no such (stable) wave phenomena exist, it is not known if strongly coupled aggregates exhibit bistable synchronous solutions. For instance, synchronous (monostable) solutions are present in heterogeneous collections of cells which are diffusively coupled with strong coupling [38].

Lastly, the approximation of the average quantity $\widehat{u}(z)$ in (2.24) is of some mathematical interest. In Figure 2.2, the functions $\widehat{u}_a(z)$ and $\widehat{u}(z)$ are shown to be very close over a wide range of z. This closeness suggests that (2.24) is a two term asymptotic approximation of the average $\widehat{u}(z)$. If this is the case, we are unaware of a systematic (analytical) method for estimating the parameters p, a_0, and a_1 in that approximation. Moreover, we are not aware how robust this approximation is when fast parameter values are altered. In Figure 2.2 the fast parameters are fixed and the comparison is over different values of z. Regardless, such approximation methods would be of interest, as they might apply to the more complicated Hodgkin–Huxley based models with two fast variables. For instance, were such methods available and the dependence of a_0 on fast parameters derivable, then it would be easier to predict how things such as the active phase duration might depend on fast conductances and other biological quantities.

Appendix. Here we use a multiple scales procedure to derive the (AFS) summarized in section 2.3. We assume that the (FS) has $T(\mathbf{z})$-periodic solutions $\Omega(t, \mathbf{z})$ which satisfy

$$\frac{d\Omega}{dt} = \mathbf{F}(\Omega, \mathbf{z}) \quad \forall \mathbf{z} \in S_A \,. \tag{A.1}$$

We seek an asymptotic approximation of (2.1)–(2.2) valid to $O(\varepsilon)$ for $t = O(\frac{1}{\varepsilon})$. Toward that end, we assume an expansion of the form

$$\mathbf{u}(t) = U(s, \tau, \varepsilon) = U_0(s, \tau) + \varepsilon U_1(s, \tau) + O(\varepsilon^2)\,, \tag{A.2}$$

$$\mathbf{z}(t) = Z(s, \tau, \varepsilon) = Z_0(s, \tau) + \varepsilon Z_1(s, \tau) + O(\varepsilon^2)\,, \tag{A.3}$$

where τ is a slow time,

$$\tau = \varepsilon t, \tag{A.4}$$

and the strained (fast) time s is defined by

$$\frac{ds}{dt} = \omega(\tau) \tag{A.5}$$

for a function ω as yet to be determined.

As with other multiple scales methods, it is possible to choose an appropriate ω so that U_0 is 1-periodic in s. In addition to the aforementioned periodicity, we want our leading-order approximation $U_0(s,\tau)$ close to $u(t)$ for times $\tau = O(1)$. With U_0 and Z_0 suitably determined, we also require $U_i(s,\tau)$ and $Z_i(s,\tau)$ to be 1-periodic in s for $i = 0, 1, 2, \ldots$. The periodicity of U_i and Z_i in s ensures the functions U, Z are bounded in s, so that, for instance, $|U - U_0| = O(\varepsilon)$ for $\tau = O(1)$.

Using these definitions, the time derivatives of $U(s,\tau,\varepsilon)$ are

$$\frac{dU}{dt} = \omega\frac{\partial U}{\partial s} + \varepsilon\frac{\partial U}{\partial \tau}\,, \tag{A.6}$$

$$\frac{d^2U}{dt^2} = \omega^2\frac{\partial^2 U}{\partial s^2} + 2\varepsilon\omega\frac{\partial^2 U}{\partial s\partial \tau} + \varepsilon\frac{\partial \omega}{\partial \tau}\frac{\partial U}{\partial s} + \varepsilon^2\frac{\partial^2 U}{\partial \tau^2}\,, \tag{A.7}$$

with similar expressions for $Z(s,\tau,\varepsilon)$.

Expanding $\mathbf{F}(\mathbf{u},\mathbf{z})$ about (U_0, Z_0) gives

$$\mathbf{F}(\mathbf{u},\mathbf{z}) = \mathbf{F}(U_0,Z_0) + \varepsilon D_{\mathbf{u}}\mathbf{F}(U_0,Z_0)U_1 + \varepsilon D_{\mathbf{z}}\mathbf{F}(U_0,Z_0)Z_1 + O(\varepsilon^2)\,, \tag{A.8}$$

where, for $\mathbf{F} = (F_1, F_2)^T$,

$$D_{\mathbf{u}}\mathbf{F} = \begin{bmatrix} \frac{\partial F_1}{\partial u} & \frac{\partial F_1}{\partial w} \\ \frac{\partial F_2}{\partial u} & \frac{\partial F_2}{\partial w} \end{bmatrix}, \tag{A.9}$$

and in a similar fashion, $D_{\mathbf{z}}\mathbf{F}$ is the Jacobian of $\mathbf{F}$ in $\mathbf{z}$.

Putting this all together, (2.1)–(2.2) become

$$\omega\frac{\partial U_0}{\partial s} + \varepsilon\left(\frac{\partial U_0}{\partial \tau} + \omega\frac{\partial U_1}{\partial s}\right) = \mathbf{F}^{(0)} + \varepsilon\left(D_{\mathbf{u}}\mathbf{F}^{(0)}U_1 + D_{\mathbf{z}}\mathbf{F}^{(0)}Z_1\right) + O(\varepsilon^2)\,, \tag{A.10}$$

$$\omega\frac{\partial Z_0}{\partial s} + \varepsilon\left(\frac{\partial Z_0}{\partial \tau} + \omega\frac{\partial Z_1}{\partial s}\right) = \varepsilon\mathbf{G}(U_0,Z_0) + O(\varepsilon^2)\,, \tag{A.11}$$

where the superscript$^{(0)}$ in (A.10) means evaluated at (U_0, Z_0). These equations can be written as a system of partial differential equations. The $O(1)$ terms from (A.10)–(A.11) are

$$\omega\frac{\partial U_0}{\partial s} = \mathbf{F}(U_0,Z_0)\,, \tag{A.12}$$

$$\frac{\partial Z_0}{\partial s} = 0\,, \tag{A.13}$$

and the $O(\varepsilon)$ terms,

$$\frac{\partial U_0}{\partial \tau} + \omega\frac{\partial U_1}{\partial s} = D_{\mathbf{u}}\mathbf{F}(U_0,Z_0)U_1 + D_{\mathbf{z}}\mathbf{F}(U_0,Z_0)Z_1\,, \tag{A.14}$$

$$\frac{\partial Z_0}{\partial \tau} + \omega\frac{\partial Z_1}{\partial s} = \mathbf{G}(U_0,Z_0)\,. \tag{A.15}$$

From (A.13) it is evident that Z_0 does not depend on s. Henceforth, we write $Z_0 = Z_0(\tau)$.

Since $\Omega(s,\mathbf{z})$ is $T(\mathbf{z})$-periodic in s, then $\Omega(Ts,\mathbf{z})$ is 1-periodic in s. Letting $\psi(\tau)$ be a slowly varying phase, then

$$U_0(s,\tau) = \Omega(sT(Z_0(\tau)) + \psi(\tau), Z_0(\tau)) \tag{A.16}$$

will also be a 1-periodic function of s. Moreover, since Ω solves (A.1), the U_0 defined in (A.16) also solves (A.12), provided we choose

$$\omega(\tau) = \frac{1}{T(Z_0(\tau))} \,. \tag{A.17}$$

With this choice of ω the strained time s is completely defined in terms of the original time t via (A.5) once $Z_0(\tau)$ has been determined. Although a subsequent determination of the dependence of U_0 on t additionally depends on the slowly varying phase ψ, it will shortly be shown that the leading-order evolution of Z_0 does not depend on ψ.

We now turn our attention to the Z equation. The requirement that Z_1 be 1-periodic in s helps us derive necessary conditions for Z_0. Integrating (A.15) over $s \in (0, 1)$, we get

$$\int_0^1 \mathbf{G}(U_0(s,\tau), Z_0(\tau))ds = \int_0^1 \left(\frac{\partial Z_0}{\partial \tau} + \omega(\tau) \frac{\partial Z_1}{\partial s}(s,\tau) \right) ds \tag{A.18}$$

$$= \frac{\partial Z_0}{\partial \tau} + \omega(\tau)[Z_1(1,\tau) - Z_1(0,\tau)] \,. \tag{A.19}$$

Thus, choosing Z_0 as a solution to

$$\frac{\partial Z_0}{\partial \tau} = \int_0^1 \mathbf{G}(U_0(s,\tau), Z_0(\tau))ds = \int_0^1 \mathbf{G}\left(\Omega(sT(Z_0) + \psi(\tau)), Z_0\right) ds \tag{A.20}$$

implies $Z_1(1, \tau) = Z_1(0, \tau)$ for all τ. This in itself does not prove that Z_1 is periodic in s. However, one need only note that (A.15) is invariant under the transformation $s \to s + \bar{\psi}$ to make this inference. Using this transformation, the preceding integration of (A.15) would then imply $Z_1(1 + \bar{\psi}, \tau) = Z_1(\bar{\psi}, \tau)$ for an arbitrary $\bar{\psi}$, from which one concludes that if Z_0 solves (A.20), then Z_1 is 1-periodic in s.

Lastly, as mentioned previously, the slowly varying phase ψ is not needed to determine the dependence of Z_0 on τ. In order to show this, we introduce the change of coordinates $\eta = sT(Z_0) + \psi(\tau)$ to rewrite (A.20) as

$$\frac{\partial Z_0}{\partial \tau} = \frac{1}{T} \int_{\psi}^{T+\psi} \mathbf{G}(\Omega(\eta, Z_0), Z_0) d\eta \,. \tag{A.21}$$

Since $\mathbf{G}(\Omega(\eta, Z_0), Z_0)$ is $T(Z_0)$-periodic in η, we have

$$\frac{\partial Z_0}{\partial \tau} = \frac{1}{T} \int_0^T \mathbf{G}(\Omega(\eta, Z_0), Z_0) d\eta \equiv \widehat{\mathbf{G}}(Z_0) \,, \tag{A.22}$$

showing that the value of the integral does not depend on $\psi(\tau)$. The right-hand equality in (A.22) has been added to emphasize that there is no explicit dependence on τ in $\widehat{G}$. Also, in summary, we may now conclude that if

$$\frac{dZ_0}{d\tau} = \widehat{\mathbf{G}}(Z_0) \,, \tag{A.23}$$

then Z_1 is 1-periodic in s so that $|Z - Z_0| = O(\varepsilon)$ for $\tau = O(1)$. Given the definition of $\mathbf{G}$ and the linearity of $h_i(u)$ in u, we see that (A.23) written out in component form is precisely (2.22)–(2.23).

REFERENCES

[1] B. Alving, *Spontaneous activity in isolated somata of Aplysia pacemaker neurons*, J. Gen. Physiol., 51 (1968), pp. 29–45.

[2] I. Atwater, C. Dawson, A. Scott, G. Eddlestone, and E. Rojas, *The nature of the oscillatory behavior in electrical activity from pancreatic β-cell*, Hormone and Metabolic Research Supplement, 10 (1980), pp. 100–107.

[3] S. Baer, J. Rinzel, and H. Carrillo, *Analysis of an autonomous phase model for neuronal parabolic bursting*, J. Math. Biol., 33 (1995), pp. 309–333.

[4] R. Bertram, M. Butte, T. Kiemel, and A. Sherman, *Topological and phenomenological classification of bursting oscillations*, Bull. Math. Biol., 57 (1995), pp. 413–439.

[5] R. Bertram, J. Previte, A. Sherman, T. Kinard, and L. Satin, *The phantom burster model for pancreatic β-cells*, Biophys. J., 79 (2000), pp. 2880–2892.

[6] R. Bertram, P. Smolen, A. Sherman, D. Mears, I. Atwater, F. Martin, and B. Soria, *A role for calcium release-activated current (CRAC) in cholinergic modulation of electrical activity in pancreatic β-cells*, Biophys. J., 68 (1995), pp. 2323–2332.

[7] W. Beyer, ed., *CRC Standard Mathematical Tables and Formulae*, 29th ed., CRC Press, Boca Raton, FL, 1991.

[8] A. Bose, N. Kopell, and D. Terman, *Almost-synchronous solutions for mutually coupled excitatory neurons*, Phys. D, 140 (2000), pp. 69–94.

[9] R. Butera, *Multirhythmic bursting*, Chaos, 8 (1998), pp. 274–284.

[10] C. C. Canavier, D. A. Baxter, J. W. Clark, and J. H. Byrne, *Nonlinear dynamics in a model neuron provide a novel mechanism for transient synaptic inputs to produce long-term alterations of postsynaptic activity*, J. Neurophysiology, 69 (1993), pp. 2252–2257.

[11] C. C. Canavier, D. A. Baxter, J. W. Clark, and J. H. Byrne, *Multiple modes of activity in a model neuron suggest a novel mechanism for the effects of neuromodulatros*, J. Neurophysiology, 72 (1994), pp. 872–882.

[12] T. Chay, *Chaos in a three-variable model of an excitable cell*, Phys. D, 16 (1985), pp. 233–242.

[13] T. Chay, *Effect of compartmentalized Ca^{2+} ions on electrical bursting activity of pancreatic β-cells*, Am. J. Physiol., 258 (1990), pp. C955–C965.

[14] T. Chay and D. Cook, *Endogenous bursting patterns in excitable cells*, Math. Biosci., 90 (1988), pp. 139–153.

[15] T. Chay and J. Keizer, *Minimal model for membrane oscillations in the pancreatic β-cell*, Biophys. J., 42 (1983), pp. 181–190.

[16] G. de Vries, *Multiple bifurcations in a polynomial model of bursting oscillations*, J. Nonlinear Sci., 8 (1998), pp. 281–316.

[17] G. de Vries, A. Sherman, and H. Zhu, *Diffusively coupled bursters: Effects of cell heterogeneity*, Bull. Math. Biol., 60 (1998), pp. 1167–1200.

[18] M. Deschênes, J. Roy, and M. Steriade, *Thalamic bursting mechanism: An inward slow current revealed by membrane hyperpolarization*, Brain Res., 239 (1982), pp. 289–293.

[19] E. J. Doedel, *AUTO: A program for the automatic bifurcation analysis of autonomous systems*, Congr. Numer., 30 (1981), pp. 265–284.

[20] E. J. Doedel and J. P. Kernevez, *AUTO: Software for Continuation and Bifurcation Problems in Ordinary Differential Equations with Applications*, Report, Department of Applied Mathematics, Caltech, Pasadena, CA, 1986.

[21] B. Ermentrout, *Simulating, Analyzing, and Animating Dynamical Systems: A Guide to XPPAUT for Researchers and Students*, SIAM, Philadelphia, 2002.

[22] L. Falke, K. Gillis, D. Pressel, and S. Misler, *Perforated patch recording allows long-term monitoring of metabolite-induced electrical activity and voltage-dependent ca^{2+} currents in pancreatic b cells*, FEBS (Fed. Eur. Biochem. Soc.) Lett., 251 (1989), pp. 167–172.

[23] R. Fitzhugh, *Impulses and physiological states in theoretical models of nerve membrane*, Biophys. J., 1 (1961), pp. 445–466.

[24] T. Gedeon, H. Kokubu, K. Mischaikow, H. Oka, and J. F. Reineck, *The Conley index for fast-slow systems.* I. *One-dimensional slow variable*, J. Dynam. Differential Equations, 11 (1999), pp. 427–470.

[25] R. E. Griffiths, *Return Map Characterizations of Singular Solutions for a Model of Bursting with Two Slow Variables*, Ph.D. thesis, Montana State University, Bozeman, MT, 2003.

[26] R. Harris-Warrick and R. Flamm, *Multiple mechanism of bursting in a conditioned bursting neuron*, J. Neurosci., 7 (1987), pp. 2113–2128.

[27] D. Himmel and T. Chay, *Theoretical studies on the electrical activity of pancreatic β-cells as a function of glucose*, Biophys. J., 51 (1987), pp. 89–107.

[28] J. Hindmarsh and R. Rose, *A model of neuronal bursting using three coupled first order differential equations*, Proc. Roy. Soc. Lond. Ser. B, 221 (1984), pp. 87–102.

[29] A. Hodgkin and A. Huxley, *A quantitative description of membrane current and its application to conduction and excitation in nerve*, J. Physiol. (Lond.), 117 (1952), pp. 500–544.

[30] E. Izhikevich, *Neural excitability, spiking, and bursting*, Inter. J. Bifur. Chaos Appl. Sci. Engrg., 10 (2000), pp. 1171–1266.

[31] J. Keizer and G. Magnus, *Atp-sensitive potassium channel and bursting in the pancreatic β cell*, Biophys. J., 56 (1989), pp. 229–242.

[32] J. Keizer and P. Smolen, *Bursting electrical activity in pancreatic β-cells caused by Ca^{2+}- and voltage-inactivated Ca^{2+} channels*, Proc. Nat. Acad. Sci. USA, 88 (1991), pp. 3897–3901.

[33] A. Kepecs and X. Wang, *Analysis of complex bursting in cortical pyramidal neuron models*, Neurocomputing, 32/33 (2000), pp. 181–187.

[34] G. S. Medvedev, *Reduction of a model of an excitable cell to a one-dimensional map*, Phys. D, 202 (2005), pp. 37–59.

[35] M. Nagumo, *A theory of degree of mapping based on infinitesimal analysis*, Amer. J. Math., 73 (1951), pp. 485–496.

[36] M. Pernarowski, *Fast subsystem bifurcations in a slowly varying Liénard system exhibiting bursting*, SIAM J. Appl. Math., 54 (1994), pp. 814–832.

[37] M. Pernarowski, *Fast and slow subsystems for a continuum model of bursting activity in the pancreatic islet*, SIAM J. Appl. Math., 58 (1998), pp. 1667–1687.

[38] M. Pernarowski, *Fast subsystem bifurcations in strongly coupled heterogeneous collections of excitable cells*, Bull. Math. Biol., 62 (2000), pp. 101–120.

[39] M. Pernarowski, R. M. Miura, and J. Kevorkian, *Perturbation techniques for models of bursting electrical activity in the pancreatic β-cell*, SIAM J. Appl. Math., 52 (1992), pp. 1627–1650.

[40] R. Plant and M. Kim, *Mathematical description of a bursting pacemaker neuron by a modification of the Hodgkin-Huxley equations*, Biophys. J., 16 (1976), pp. 227–244.

[41] J. Rinzel, *A formal classification of bursting mechanisms in excitable systems*, in Mathematical Topics in Population Biology, Morphogenesis, and Neurosciences, E. Teramato and M. Yamaguti, eds., Lecture Notes in Biomath. 71, Springer-Verlag, Berlin, 1987, pp. 267–281.

[42] P. Rorsman and G. Trube, *Calcium and delayed potassium currents in mouse pancreatic β-cells under voltage-clamp conditions*, J. Physiol. (Lond.), 374 (1986), pp. 531–550.

[43] A. Sherman, *Anti-phase, asymmetric, and aperiodic oscillations in excitable cells*—I. *Coupled bursters*, Bull. Math. Biol., 56 (1994), pp. 811–835.

[44] A. Sherman, *Case Studies in Mathematical Modeling—Ecology, Physiology, and Cell Biology*, Prentice-Hall, Upper Saddle River, NJ, 1997.

[45] A. Sherman and J. Rinzel, *Model for synchronization of pancreatic β-cells by gap junctions*, Biophys. J., 59 (1991), pp. 547–559.

[46] A. Sherman, J. Rinzel, and J. Keizer, *Emergence of organized bursting in clusters of pancreatic β-cells by channel sharing*, Biophys. J., 54 (1988), pp. 411–425.

[47] A. Shilnikov, R. Calabrese, and G. Cymbalyuk, *Mechanism of bistability: Tonic spiking and bursting in a neuron model*, Phys. Rev. E, 71 (2005), p. 056214.

[48] P. Smith, F. Aschroft, and P. Rorsman, *Simultaneous recordings of glucose dependent electrical activity and atp-regulated k^+-currents in isolated mouse pancreatic β-cells*, FEBS (Fed. Eur. Biochem. Soc.) Lett., 261 (1990), pp. 187–190.

[49] P. Smolen and J. Keizer, *Slow voltage-inactivation of Ca^{2+} currents and bursting mechanisms for the mouse pancreatic β-cell*, J. Memb. Biol., 127 (1992), pp. 9–19.

[50] P. Smolen, J. Rinzel, and A. Sherman, *Why pancreatic islets burst but single β-cells do not: The heterogeneity hypothesis*, Biophys. J., 64 (1993), pp. 1668–1680.

[51] P. Smolen, D. Terman, and J. Rinzel, *Properties of a bursting model with two slow inhibitory variables*, SIAM J. Appl. Math., 53 (1993), pp. 861–892.

[52] F. Strumwasser, *Types of information stored in single neurons*, in Invertebrate Nervous Systems: Their Significance for Mammalian Neurophysiology, C. Wiersma, ed., The University of Chicago Press, Chicago, 1967, pp. 290–319.

[53] D. Terman, *Chaotic spikes arising from a model of bursting in excitable membranes*, SIAM J. Appl. Math., 51 (1991), pp. 1418–1450.

[54] D. Terman, *The transition from bursting to continuous spiking in excitable membrane models*, J. Nonlinear Sci., 2 (1992), pp. 135–182.

[55] X. Wang, *Fast burst firing and short-term synaptic plasticity: A model of neocortical chattering neurons*, Neurosci., 89 (1999), pp. 347–362.

[56] R. Wong and D. Prince, *Afterpotential generation in hippocampal pyramidal cells*, J. Neurophysiol., 45 (1981), pp. 86–97.